

Even-Odd and Super-Even Effects in the Attractive Hubbard Model

K. Tanaka and F. Marsiglio

Department of Physics, University of Alberta, Edmonton, Alberta, Canada T6G 2J1

(August 9, 2018)

The canonical BCS wave function is tested for the attractive Hubbard model. Results are presented for one dimension, and are compared with the exact solutions by the Bethe ansatz and the results from the conventional grand canonical BCS approximation, for various chain lengths, electron densities, and coupling strengths. While the exact ground state energies are reproduced very well both by the canonical and grand canonical BCS approximations, the canonical method significantly improves the energy gaps for small systems and weak coupling. The “parity” effect due to the number of electrons being even or odd naturally emerges in our canonical results. Furthermore, we find a “super-even” effect: the energy gap oscillates as a function of even electron number, depending on whether the number of electrons is $4m$ or $4m + 2$ (m integer). Such oscillations as a function of electron number should be observable with tunneling measurements in ultra-small metallic grains.

PACS number(s): 74.20.Fg, 71.24.+q, 71.10.Fd, 71.10.Li

I. INTRODUCTION

The possibility of fabricating [1] tunnel junctions containing nanoscale particles has opened up new areas of exploration. Experiments can now probe the energy spectrum in these particles and study changes as a function of temperature and magnetic field [2,3]. In this way one can observe changes in the spectrum that are expected to occur in the bulk due to phase transitions, and determine to what extent these concepts are relevant for small systems [4]. The unprecedented control over experimental conditions — changes due to a single tunneling electron can be observed — allows one to ask and address questions which, until now, have been academic only.

In this study we follow the experiments of Tinkham *et al.* [1–3] and address the issues concerning superconductivity in small systems. Specifically they studied small superconducting Al particles (diameter of order 10 nm) and probed, through tunneling experiments, the excitation spectrum as a function of temperature and magnetic field. In attempting to treat small electronic systems, there are many concerns related to possible surface and impurity effects, both of which could lead to localization, for example. For the present we ignore these potential complications, and instead focus on a question which arises in the application of the Bardeen-Cooper-Schrieffer (BCS) [5] theory of superconductivity: to what extent is the grand canonical ensemble useful (which in the ther-

modynamic limit, is equivalent to the canonical one) for systems with a small number of electrons?

We propose to tackle this question in a systematic way, using the attractive Hubbard model. The choice of this model is motivated by several factors. It has long served as a paradigm for s-wave superconductivity, and serves as the ‘minimal’ model that best describes superconductivity. All the energy scales are very well defined in the problem, so that no high frequency (and ill-defined) cut-offs are required [6]. Exact solutions are available in one dimension via Bethe Ansatz techniques [7], and the grand canonical BCS solutions have recently been evaluated for large system sizes [8]. In fact in that work some preliminary canonical solutions were also examined, but only for very small system sizes. In this work we reformulate the canonical solution, in such a way that larger systems up to three dimensions can be tackled. We note that after this work was completed, a paper appeared [9] in which the canonical BCS equations were formulated and solved for a model system with uniformly spaced level spacings. We will comment on the similarities and differences with our own work in the course of our discussion below.

The outline of the paper is as follows. In the next section we formulate the problem. We mention the work of Falicov and Proetto [10], who applied a canonical BCS method to the problem of electrons on a tetrahedron (a ‘small’ fcc lattice). We have generalized this method for larger systems, and solved the ensuing equations numerically. However, memory requirements become very demanding, and therefore, beyond a certain lattice size, we had to abandon this approach. We include it in the appendix, nonetheless, because the variational wave function in this method is more general than the BCS canonical wave function, and the variational equation is linear. In practice, however, as will be shown, this wave function only marginally improves the ground state energy.

We then formulate the canonical variational problem strictly in terms of the $g(\mathbf{k})$ ’s familiar from the grand canonical solution [11]. The resulting equations are tedious, and can be cast in a more enlightening form by following the pioneering work of Dietrich, Mang and Pradal [12], who solved the canonical BCS problem for nuclei. This “method of residues” is based on representing expectation values in the BCS canonical ensemble through contour integrals of the BCS grand canonical ensemble expectation values: the latter seems to have started with a paper by Bayman [13]. This is also the methodology adopted by Braun and von Delft [9], who numerically evaluated residue integrals by fast Fourier transform. As

will be explained, however, we chose to evaluate the required integrals analytically (which requires numerical summations). A concise summary of the residue method and further references are available in Ref. [14].

Finally, we provide a review of the grand canonical formulation and the Bethe Ansatz solutions in one dimension [7,15,8], for purposes of comparison. We have also performed some numerical diagonalizations, although these are limited to small systems and (in one dimension) serve only to verify the Bethe Ansatz solutions. In both the grand canonical and canonical BCS formulations we have performed the variation strictly in terms of the single set of parameters, $g(\mathbf{k})$. This departs from more conventional treatments where two sets of parameters, $u(\mathbf{k})$, and $v(\mathbf{k})$, are used, with an auxiliary relation between them. Our formulation is conceptually clearer, but slightly more cumbersome, so some details are provided.

The following section is devoted to numerical results. All the computational results presented in this paper will be in one dimension. This is because the exact results for ‘large’ systems are only available in 1-D, and therefore it is presently only in this case that one can study the full crossover from the bulk limit to small systems. Because the attractive Hubbard model is a very local model, many of the features of the variational solution will remain in higher dimension; in fact we expect the agreement of the canonical BCS results with the exact ones to improve, but we have no way at present to check this. In addition, many of the features of the solutions in higher dimensions (such as long range order) will not be present in one dimension. A more systematic study of the canonical BCS solution in two and three dimensions will be presented elsewhere (unfortunately without exact checks, except for very small systems).

Aside from evaluations of the canonical BCS formulation we will demonstrate the so-called ‘parity effect’ [16,17], where qualitative differences in the tunneling gap can be observed, depending on whether an even or odd number of electrons occupies the small Al particle. While this has been understood within a parity-conserved grand canonical BCS formulation [18], it becomes much clearer in a canonical formulation. In addition we have found an interesting $4m$ vs. $4m + 2$ effect, where m is an integer. In our case we have observed oscillations as a function of electron number. Therefore we have variations in the gap between odd, even and *super-even* (i.e. multiples of 4) electrons. Hints of such behaviour, noted as a function of *lattice size*, were first discussed by Fye *et al.* [19].

The concluding section summarizes our results. In the Appendix we outline the formulation of the linearized canonical variation.

II. FORMULATION

A. Model

The attractive Hubbard Hamiltonian is given by

$$H = - \sum_{i,\delta} t_\delta (a_{i+\delta,\sigma}^\dagger a_{i\sigma} + \text{h.c.}) - |U| \sum_i n_{i\uparrow} n_{i\downarrow} \quad (1a)$$

$$= \sum_{\mathbf{k}\sigma} \epsilon_{\mathbf{k}} a_{\mathbf{k}\sigma}^\dagger a_{\mathbf{k}\sigma} - \frac{|U|}{N} \sum_{\mathbf{k}\mathbf{k}'\mathbf{q}} a_{\mathbf{k}\uparrow}^\dagger a_{-\mathbf{k}+\mathbf{q}\downarrow}^\dagger a_{-\mathbf{k}'+\mathbf{q}\downarrow} a_{\mathbf{k}'\uparrow}, \quad (1b)$$

where $a_{i\sigma}^\dagger$ ($a_{i\sigma}$) creates (annihilates) an electron with spin σ at site i and $n_{i\sigma}$ is the number operator for an electron with spin σ at site i (i is the index for the primitive vector \mathbf{R}_i). The t_δ is the hopping rate of electrons from one site to a neighbouring site \mathbf{R}_δ away (often nearest neighbours only are included), and $|U|$ is the coupling strength between electrons on the same site; here the fact that it is attractive is explicitly included from the beginning. In Eq. (1b), we have Fourier transformed the Hamiltonian with periodic boundary conditions for N sites in each dimension. The $a_{\mathbf{k}\sigma}^\dagger$ and $a_{\mathbf{k}\sigma}$ are the creation and annihilation operators in the reciprocal space, and the kinetic energy is given by

$$\epsilon_{\mathbf{k}} = -2 \sum_{\delta} t_\delta \cos \mathbf{k} \cdot \mathbf{R}_\delta, \quad (2)$$

where \mathbf{R}_δ is the coordinate vector connecting sites i to $i + \delta$.

We perform variational calculations using the component of the BCS wave function that has a given number of pairs ν and thus conserves the number of electrons $N_e = 2\nu$. The BCS wave function is a superposition of pair states with all the possible numbers of pairs $\{\nu\}$:

$$|\text{BCS}\rangle_{\text{GC}} = \prod_{\mathbf{k}} (u_{\mathbf{k}} + v_{\mathbf{k}} a_{\mathbf{k}\uparrow}^\dagger a_{-\mathbf{k}\downarrow}^\dagger) |0\rangle \equiv \sum_{\nu=0}^{\infty} |\Psi_{2\nu}\rangle, \quad (3)$$

where $|0\rangle$ denotes the vacuum state, and $|\Psi_0\rangle \equiv |0\rangle$. The ν -pair component $|\Psi_{2\nu}\rangle$ can be obtained by rearranging $|\text{BCS}\rangle_{\text{GC}}$ into a power series of the pair creation operator $a_{\mathbf{k}\uparrow}^\dagger a_{-\mathbf{k}\downarrow}^\dagger$ and can be written as

$$\begin{aligned} |\Psi_{2\nu}\rangle &= \sum_{\mathbf{k}_1 < \mathbf{k}_2 < \dots < \mathbf{k}_\nu} \prod_{i=1}^{\nu} \left(g(\mathbf{k}_i) a_{\mathbf{k}_i\uparrow}^\dagger a_{-\mathbf{k}_i\downarrow}^\dagger \right) |0\rangle \quad (4) \\ &= \frac{1}{\nu!} \prod_{i=1}^{\nu} \left(\sum_{\mathbf{k}_i} g(\mathbf{k}_i) a_{\mathbf{k}_i\uparrow}^\dagger a_{-\mathbf{k}_i\downarrow}^\dagger \right) |0\rangle \\ &\quad (\mathbf{k}_i \neq \mathbf{k}_j, \text{ for all } i \neq j). \quad (4') \end{aligned}$$

Here we have defined $g(\mathbf{k}_i) = \left(\prod_{\mathbf{k}} u_{\mathbf{k}} \right)^{1/\nu} v_{\mathbf{k}_i}/u_{\mathbf{k}_i}$. The condition $\mathbf{k}_1 < \mathbf{k}_2 < \dots < \mathbf{k}_\nu$ for the $\{\mathbf{k}_i\}$ sums in Eq. (4) means that all the \mathbf{k}_i 's should be different and ordered so that all the different combinations of $\{\mathbf{k}_i\}$ are counted once each: the latter condition is removed for

the sums in Eq. (4') and the division by $\nu!$ compensates for the multiple counting. In a finite system with N sites in each dimension, the wave number can take N^D values, where D is the dimension of the system, and hence the ν sums over \mathbf{k} 's in Eq. (4) result in ${}_{N^D}C_\nu = \frac{N^D!}{\nu!(N^D-\nu)!}$ terms.

B. Grand Canonical Variation

We begin by reviewing the grand canonical formulation of BCS theory. We have opted, contrary to convention, to formulate the minimization problem in terms of only the variational parameters, $g_{\mathbf{k}} \equiv g(\mathbf{k})$ (and not the $u_{\mathbf{k}}$'s and $v_{\mathbf{k}}$'s). This was originally motivated by the loss of clear meaning for the $u_{\mathbf{k}}$'s and $v_{\mathbf{k}}$'s in the canonical ensemble, though in fact one can proceed equally well with these [12,9]. One therefore simply writes:

$$|\text{BCS}\rangle_{\text{GC}} = c \prod_{\mathbf{k}} (1 + g_{\mathbf{k}} a_{\mathbf{k}\uparrow}^\dagger a_{-\mathbf{k}\downarrow}^\dagger) |0\rangle, \quad (5)$$

where the coefficient c properly normalizes the wave function. One then calculates the various expectation values to determine the ground state energy:

$$E = \frac{\langle \Psi | H | \Psi \rangle}{\langle \Psi | \Psi \rangle}, \quad (6)$$

where, in this case, the wave function is the BCS grand canonical one given in Eq. (5). For example, the expectation value of the kinetic energy operator, \hat{T} is

$$\langle \Psi | \hat{T} | \Psi \rangle = 2 |c|^2 \prod_{\mathbf{p}} (1 + g_{\mathbf{p}}^2) \sum_{\mathbf{k}} (\epsilon_{\mathbf{k}} - \mu) \frac{g_{\mathbf{k}}^2}{1 + g_{\mathbf{k}}^2}. \quad (7)$$

Note that normally the product and the denominator are absent because these factors are normally defined to be unity due to normalization. Also note that the $g_{\mathbf{k}}$'s are generally complex, but can be chosen to be real; this is presumed in Eq. (7), and will be implicit in what follows. Careful evaluation of the potential energy terms yields the following result:

$$E_{\text{GC}} = 2 \sum_{\mathbf{k}} (\epsilon_{\mathbf{k}} - \mu) \frac{g_{\mathbf{k}}^2}{1 + g_{\mathbf{k}}^2} - \frac{|U|}{N} \sum_{\mathbf{k}} \frac{g_{\mathbf{k}}^2}{1 + g_{\mathbf{k}}^2} - \frac{|U|}{N} \sum_{\mathbf{k} \neq \mathbf{k}'} \frac{g_{\mathbf{k}}}{1 + g_{\mathbf{k}}^2} \frac{g_{\mathbf{k}'}}{1 + g_{\mathbf{k}'}^2} - \frac{|U|}{N} \sum_{\mathbf{k} \neq \mathbf{k}'} \frac{g_{\mathbf{k}}^2}{1 + g_{\mathbf{k}}^2} \frac{g_{\mathbf{k}'}}{1 + g_{\mathbf{k}'}^2} \quad (8)$$

with μ the chemical potential; it plays the mathematical role of the Lagrange multiplier for the condition that the average electron number ${}_{\text{GC}}\langle \text{BCS} | \hat{N}_e | \text{BCS} \rangle_{\text{GC}} = N_e$. We have written the total energy term by term in the following sequence: the first term is the kinetic energy, the following two come from Cooper pair scattering ($\mathbf{q} = 0$), and the fourth term is the Hartree term ($\mathbf{q} \neq 0$). When

displayed this way it is apparent that the last term excludes the spurious Hartree term whereby an electron interacts with itself (a '1/N effect'). It is also apparent that the *reduced* BCS Hamiltonian ($\mathbf{q} = 0$ scattering only) will exclude this last term, and in doing so omits the Hartree term (since it is often deemed to merely represent a shift in energies). At the same time Eq. (8) appears to have terms of order 1/N smaller than the dominant terms. In fact it does not, and we can rewrite this equation in the following form:

$$E_{\text{GC}} = 2 \sum_{\mathbf{k}} (\epsilon_{\mathbf{k}} - \mu) \frac{g_{\mathbf{k}}^2}{1 + g_{\mathbf{k}}^2} - \frac{|U|}{N} \sum_{\mathbf{k}, \mathbf{k}'} \left[\frac{g_{\mathbf{k}}}{1 + g_{\mathbf{k}}^2} \frac{g_{\mathbf{k}'}}{1 + g_{\mathbf{k}'}^2} + \frac{g_{\mathbf{k}}^2}{1 + g_{\mathbf{k}}^2} \frac{g_{\mathbf{k}'}}{1 + g_{\mathbf{k}'}^2} \right], \quad (9)$$

where now the summations are unrestricted. The entire expression is now clearly extensive, as it should be, though in this form *pairing* terms of order 1/N have been mixed in with the Hartree term.

The next step is to carry out the variation with respect to the $g_{\mathbf{k}}$'s; this can be done straightforwardly to yield:

$$2 (\epsilon_{\mathbf{k}} - \tilde{\mu}) g_{\mathbf{k}} = \frac{|U|}{N} \sum_{\mathbf{k}'} \frac{g_{\mathbf{k}'}}{1 + g_{\mathbf{k}'}^2} [1 - g_{\mathbf{k}}^2], \quad (10)$$

where

$$\tilde{\mu} \equiv \mu + \frac{|U|}{N} \sum_{\mathbf{k}} \frac{g_{\mathbf{k}}^2}{1 + g_{\mathbf{k}}^2}. \quad (11)$$

We also define the pair potential,

$$\Delta_{\text{BCS}} \equiv \frac{|U|}{N} \sum_{\mathbf{k}} \frac{g_{\mathbf{k}}}{1 + g_{\mathbf{k}}^2} \quad (12)$$

so that the BCS equation can be written

$$2 (\epsilon_{\mathbf{k}} - \tilde{\mu}) g_{\mathbf{k}} = \Delta_{\text{BCS}} [1 - g_{\mathbf{k}}^2]. \quad (13)$$

The solution is

$$g_{\mathbf{k}} = \frac{E_{\mathbf{k}} - (\epsilon_{\mathbf{k}} - \tilde{\mu})}{\Delta_{\text{BCS}}}, \quad (14)$$

where $E_{\mathbf{k}} \equiv \sqrt{(\epsilon_{\mathbf{k}} - \tilde{\mu})^2 + \Delta_{\text{BCS}}^2}$ is the quasi-particle energy. This solution is only implicit, since Δ_{BCS} depends on the $g_{\mathbf{k}}$'s through Eq. (12), and must be determined by numerical iteration. The number equation is also required to determine the chemical potential as a function of coupling strength. It is [11]

$$n \equiv \frac{\langle N_e \rangle}{N} = 1 - \frac{1}{N} \sum_{\mathbf{k}} \frac{(\epsilon_{\mathbf{k}} - \tilde{\mu})}{E_{\mathbf{k}}}. \quad (15)$$

The gap is then defined to be

$$\Delta_{\circ} = \min (E_{\mathbf{k}}). \quad (16)$$

If we define the minimum band energy, $\epsilon_{\min} \equiv -D/2$, with D the bandwidth, then it follows that $\Delta_{\circ} = \sqrt{(\epsilon_{\min} - \tilde{\mu})^2 + \Delta_{\text{BCS}}^2}$ when $\tilde{\mu} < \epsilon_{\min}$. This definition implies that the gap depends on a certain momentum, determined by the wave vector \mathbf{k} at which the minimum energy occurs. The total energy also follows readily from these expressions. It is

$$\frac{E_{\text{GC}}}{N} = \frac{1}{N} \sum_{\mathbf{k}} \epsilon_{\mathbf{k}} \left(1 - \frac{\epsilon_{\mathbf{k}} - \tilde{\mu}}{E_{\mathbf{k}}} \right) - |U| \left(\frac{n}{2} \right)^2 - \frac{\Delta_{\text{BCS}}^2}{|U|}, \quad (17)$$

where we have used the fact that $n = \frac{2}{N} \sum_{\mathbf{k}} \frac{g_{\mathbf{k}}^2}{1+g_{\mathbf{k}}^2}$. The BCS grand canonical results in the remainder of the paper have been obtained through the solution of these equations on finite lattices.

C. Canonical Variation

1. BCS

Rather than adopt the wave function given by Eq. (5), which spans all (even) number sectors, one can work directly with the wave function $|\Psi_{2\nu}\rangle$ given by Eq. (4) with fixed electron number, $N_e = 2\nu$. A ‘simplification’ occurs if we try to linearize the problem, by defining a variational parameter $C(\mathbf{k}_1, \mathbf{k}_2, \dots, \mathbf{k}_{\nu}) \equiv g(\mathbf{k}_1)g(\mathbf{k}_2)\dots g(\mathbf{k}_{\nu})$ for this wave function, following Refs. [10] and [8] for the two-pair case. Thus one can rewrite Eq. (4) as

$$|\Psi_{2\nu}\rangle = \sum_{\mathbf{k}_1 < \mathbf{k}_2 < \dots < \mathbf{k}_{\nu}} C(\mathbf{k}_1, \mathbf{k}_2, \dots, \mathbf{k}_{\nu}) \prod_{i=1}^{\nu} a_{\mathbf{k}_i \uparrow}^{\dagger} a_{-\mathbf{k}_i \downarrow}^{\dagger} |0\rangle. \quad (18)$$

As discussed in Ref. [10], the C ’s defined as above are subject to constraints; for example, for $\nu = 2$ and for a given set of four \mathbf{k} values ($\mathbf{q}_1, \mathbf{q}_2, \mathbf{q}_3, \mathbf{q}_4$) which satisfy $\mathbf{q}_1 < \mathbf{q}_2 < \mathbf{q}_3 < \mathbf{q}_4$,

$$\begin{aligned} C(\mathbf{q}_1, \mathbf{q}_2) C(\mathbf{q}_3, \mathbf{q}_4) &= C(\mathbf{q}_1, \mathbf{q}_3) C(\mathbf{q}_2, \mathbf{q}_4) \\ &= C(\mathbf{q}_1, \mathbf{q}_4) C(\mathbf{q}_2, \mathbf{q}_3). \end{aligned} \quad (19)$$

If these constraints are ignored and the C ’s in Eq. (18) are treated as $N^{\nu} C_{\nu}$ independent parameters, the minimization of the energy

$$E_{2\nu} = \frac{\langle \Psi_{2\nu} | H | \Psi_{2\nu} \rangle}{\langle \Psi_{2\nu} | \Psi_{2\nu} \rangle} \quad (20)$$

with respect to $\{C\}$ reduces to a linear problem [10]. We initially adopted this method of canonical variation, which actually allows more variational freedom than using the $g_{\mathbf{k}}$ ’s. However, as one can readily appreciate,

the number of variational parameters grows very quickly with increasing lattice size, and therefore in practice, this method has limited usage. Where it was practical, however, we carried out these calculations and compared them with the canonical BCS results to be described below. The gain in accuracy for the ground state energy was fairly small. Our formulation and results in this case are summarized in the Appendix.

The cost of working with the $g_{\mathbf{k}}$ ’s is that the problem remains a very nonlinear one. Nonetheless the gain in computational ease more than compensates for this, in that only N variational parameters are required, where N is the number of lattice sites. As we shall see, this allows us to easily study the limit from small systems to those that are well described by the grand canonical ensemble. The formulation of this problem using the expression for $|\Psi_{2\nu}\rangle$ given in Eq. (4) is straightforward but tedious. We therefore follow the ‘method of residues’ [12] (see also [14] and more recently [9]) originally developed for the nuclear pairing problem. An advantage of this method is that matrix elements are more easily evaluated (they remain as simple as the ones in the grand canonical formulation). Moreover the energy and the resulting variational equation can be written in a compact way which parallels the grand canonical BCS equations. The starting point is to write Eq. (4) in the general form as a particle-number projection of the grand canonical BCS state [13]. In more general terms, this is the projection that restores the symmetry of the Hamiltonian (i.e., conserved particle number in this case) in the wave function [14,20].

For an even number of electrons the ν -pair wave function in the projected form is

$$|\Psi_{2\nu}\rangle = \frac{1}{2\pi i} \oint d\xi \xi^{-\nu-1} \prod_{\mathbf{k}} \left(1 + \xi g_{\mathbf{k}} a_{\mathbf{k}\uparrow}^{\dagger} a_{-\mathbf{k}\downarrow}^{\dagger} \right) |0\rangle, \quad (21)$$

where the contour is any counterclockwise path that encloses the origin. If we perform the residue integral above, we recover the desired wave function Eq. (4).

As written above the wave function is not normalized, so expectation values of observables will include a factor given by $\langle \Psi_{\nu} | \Psi_{\nu} \rangle$ in the denominator. A straightforward evaluation of this factor gives $\langle \Psi_{\nu} | \Psi_{\nu} \rangle = R_0^0$, where R_n^m is defined by the residue integral [12]

$$\begin{aligned} R_n^m(\mathbf{k}_1, \mathbf{k}_2, \dots, \mathbf{k}_m) &= \frac{1}{2\pi i} \oint d\xi \xi^{-(\nu-n)-1} \prod_{\mathbf{k} \neq \mathbf{k}_1, \mathbf{k}_2, \dots, \mathbf{k}_m} (1 + \xi g_{\mathbf{k}}^2) \end{aligned} \quad (22)$$

$$= \sum_{\mathbf{p}_1 < \mathbf{p}_2 < \dots < \mathbf{p}_{\nu-n}} g_{\mathbf{p}_1}^2 g_{\mathbf{p}_2}^2 \dots g_{\mathbf{p}_{\nu-n}}^2, \quad (23)$$

where $\mathbf{p}_i \neq \mathbf{k}_1, \mathbf{k}_2, \dots, \mathbf{k}_m$ ($i = 1, \dots, \nu - n$).

The integral in Eq. (22) has sharp oscillations as a function of ξ (or θ defined by the coordinate transformation $\xi = e^{i\theta}$) whose severity increases with increasing system size. We therefore evaluated the integral using the analytical result Eq. (23). This was accomplished efficiently with an algorithm that took advantage of the polynomial structure of the original integrand in (22), and led to a considerable speed up in the integral evaluations.

These residue integrals are useful not only because the matrix elements can be easily evaluated, but also because they satisfy various recursion and sum formulas. For example, Dietrich *et al.* [12] found the following recursion relation

$$R_n^m(\mathbf{k}_1, \mathbf{k}_2, \dots, \mathbf{k}_m) = R_n^{m+1}(\mathbf{k}_1, \mathbf{k}_2, \dots, \mathbf{k}_m, \mathbf{k}) + g_{\mathbf{k}}^2 R_{n+1}^{m+1}(\mathbf{k}_1, \mathbf{k}_2, \dots, \mathbf{k}_m, \mathbf{k}). \quad (24)$$

This result follows straightforwardly from the definition. Another useful relation involves the derivative required in the variational principle:

$$\frac{\partial R_n^m(\mathbf{k}_1, \mathbf{k}_2, \dots, \mathbf{k}_m)}{\partial g_{\mathbf{k}}} = 2 g_{\mathbf{k}} R_{n+1}^{m+1}(\mathbf{k}_1, \mathbf{k}_2, \dots, \mathbf{k}_m, \mathbf{k}). \quad (25)$$

In addition, we have also found and exploited the following sum rule:

$$\sum_{\mathbf{k} \neq \mathbf{k}_1, \mathbf{k}_2, \dots, \mathbf{k}_m} g_{\mathbf{k}}^2 R_{n+1}^{m+1}(\mathbf{k}_1, \mathbf{k}_2, \dots, \mathbf{k}_m, \mathbf{k}) = (\nu - n) R_n^m(\mathbf{k}_1, \mathbf{k}_2, \dots, \mathbf{k}_m) \quad (\nu > n). \quad (26)$$

All these relations follow in a very straightforward fashion from the definition. For completeness we include the case where the residue with two or more equal indices is required; it is then useful to rewrite the definition of the residue, Eq. (22) as

$$R_n^m(\mathbf{k}_1, \mathbf{k}_2, \dots, \mathbf{k}_m) = \frac{1}{2\pi i} \oint d\xi \xi^{-(\nu-n)-1} \frac{\prod_{\mathbf{k}} (1 + \xi g_{\mathbf{k}}^2)}{\prod_{\mathbf{k}=\mathbf{k}_1, \mathbf{k}_2, \dots, \mathbf{k}_m} (1 + \xi g_{\mathbf{k}}^2)}. \quad (27)$$

The advantage of this definition over Eq. (22) is that there is no ambiguity when one or more momentum index is used more than once. With this definition these residues still satisfy the recursion relation (24). This fact is useful for simplifying the expressions that involve restricted double momentum sums, which arise in the canonical formulation.

Omitting details, the ground state energy can be written in a form reminiscent of the grand canonical BCS formulation (see Eq. (9)):

$$E_{2\nu} = \sum_{\mathbf{k}} 2 \epsilon_{\mathbf{k}} \frac{g_{\mathbf{k}}^2}{1 + g_{\mathbf{k}}^2} r_1^1(\mathbf{k})$$

$$- \frac{|U|}{N} \sum_{\mathbf{k}, \mathbf{k}'} \left[\frac{g_{\mathbf{k}}}{1 + g_{\mathbf{k}}^2} \frac{g_{\mathbf{k}'}}{1 + g_{\mathbf{k}'}^2} r_1^2(\mathbf{k}, \mathbf{k}') + \frac{g_{\mathbf{k}}^2}{1 + g_{\mathbf{k}}^2} \frac{g_{\mathbf{k}'}}{1 + g_{\mathbf{k}'}^2} r_2^2(\mathbf{k}, \mathbf{k}') \right], \quad (28)$$

where we have now defined normalized residues:

$$r_n^m(\mathbf{k}_1, \dots, \mathbf{k}_m) \equiv \frac{R_n^m(\mathbf{k}_1, \dots, \mathbf{k}_m)}{R_0^0} \prod_{\mathbf{k}'=\mathbf{k}_1, \dots, \mathbf{k}_m} (1 + g_{\mathbf{k}'}^2). \quad (29)$$

This definition is clearly motivated by the fact that in the bulk limit, the canonical results converge to the grand canonical ones.

A straightforward but tedious variation of Eq. (28) yields the following variational equation:

$$(2\tilde{\epsilon}_{\mathbf{k}} + \Lambda_{\mathbf{k}}) g_{\mathbf{k}} = \Delta_{\mathbf{k}} [1 - g_{\mathbf{k}}^2], \quad (30)$$

where

$$\tilde{\epsilon}_{\mathbf{k}} \equiv \epsilon_{\mathbf{k}} r_1^1(\mathbf{k}) - \frac{|U|}{N} \sum_{\mathbf{k}'} \frac{g_{\mathbf{k}'}}{1 + g_{\mathbf{k}'}^2} r_2^2(\mathbf{k}', \mathbf{k}) \quad (31)$$

$$\Delta_{\mathbf{k}} \equiv \frac{|U|}{N} \sum_{\mathbf{k}'} \frac{g_{\mathbf{k}'}}{1 + g_{\mathbf{k}'}^2} r_1^2(\mathbf{k}', \mathbf{k}) \quad (32)$$

$$\begin{aligned} \Lambda_{\mathbf{k}} \equiv & 2 \epsilon_{\mathbf{k}} g_{\mathbf{k}}^2 r_1^1(\mathbf{k}) [1 - r_1^1(\mathbf{k})] \\ & + \frac{|U|}{N} \left\{ r_1^1(\mathbf{k})(1 - g_{\mathbf{k}}^2) - r_1^2(\mathbf{k}, \mathbf{k}) \right\} \\ & + (1 + g_{\mathbf{k}}^2) \sum_{\mathbf{k}' \neq \mathbf{k}} 2 \epsilon_{\mathbf{k}'} \frac{g_{\mathbf{k}'}}{1 + g_{\mathbf{k}'}^2} \left(r_2^2(\mathbf{k}', \mathbf{k}) - r_1^1(\mathbf{k}) r_1^1(\mathbf{k}') \right) \\ & - 2 \frac{|U|}{N} g_{\mathbf{k}} \sum_{\mathbf{k}' \neq \mathbf{k}} \frac{g_{\mathbf{k}'}}{1 + g_{\mathbf{k}'}^2} \left(r_1^2(\mathbf{k}', \mathbf{k}) + g_{\mathbf{k}'} g_{\mathbf{k}'} r_2^2(\mathbf{k}', \mathbf{k}) \right) \\ & - \frac{|U|}{N} (1 + g_{\mathbf{k}}^2) \sum_{\mathbf{p}, \mathbf{p}' \neq \mathbf{k}} \frac{g_{\mathbf{p}}}{1 + g_{\mathbf{p}}^2} \frac{g_{\mathbf{p}'}}{1 + g_{\mathbf{p}'}^2} \left[r_3^2(\mathbf{p}, \mathbf{p}', \mathbf{k}) \right. \\ & \quad \left. + g_{\mathbf{p}} g_{\mathbf{p}'} r_3^3(\mathbf{p}, \mathbf{p}', \mathbf{k}) \right] \\ & + \frac{|U|}{N} (1 + g_{\mathbf{k}}^2) r_1^1(\mathbf{k}) \sum_{\mathbf{p}, \mathbf{p}'} \frac{g_{\mathbf{p}}}{1 + g_{\mathbf{p}}^2} \frac{g_{\mathbf{p}'}}{1 + g_{\mathbf{p}'}^2} \left[r_1^2(\mathbf{p}, \mathbf{p}') \right. \\ & \quad \left. + g_{\mathbf{p}} g_{\mathbf{p}'} r_2^2(\mathbf{p}, \mathbf{p}') \right] \end{aligned} \quad (33)$$

A solution to Eq. (30) is obtained by numerical iteration. Note that Eq. (30) resembles the analogous equation in the grand canonical ensemble, Eq. (13). The factor $\Lambda_{\mathbf{k}}$ appears here in addition; all terms in Eq. (33) are of order $1/N$, and therefore vanish in the thermodynamic limit. Moreover, both the single-particle energy Eq. (31) and the pairing potential Eq. (32) are modified by the normalized residue integrals. In practice, instead of Eqs. (30)-(33), we used the simpler-looking expression:

$$g_{\mathbf{k}} = -\frac{|U|}{N} \frac{\sum_{\mathbf{p} \neq \mathbf{k}} R_1^2(\mathbf{k}, \mathbf{p})}{\text{denom}}, \quad \text{where}$$

$$\begin{aligned} \text{denom} = & \left(E_{2\nu} - 2\epsilon_{\mathbf{k}} + \frac{|U|}{N} \right) R_1^1(\mathbf{k}) \\ & - \sum_{\mathbf{p} \neq \mathbf{k}} \left(2\epsilon_{\mathbf{p}} - 3\frac{|U|}{N} \right) g_{\mathbf{p}}^2 R_2^2(\mathbf{k}, \mathbf{p}) \\ & + \frac{|U|}{N} \sum_{\mathbf{p} \neq \mathbf{k}} \sum_{\mathbf{p}' \neq \mathbf{k}, \mathbf{p}' \neq \mathbf{p}} \left[g_{\mathbf{p}} g_{\mathbf{p}'} R_2^3(\mathbf{k}, \mathbf{p}, \mathbf{p}') \right. \\ & \left. + g_{\mathbf{p}}^2 g_{\mathbf{p}'}^2 R_3^3(\mathbf{k}, \mathbf{p}, \mathbf{p}') \right]. \end{aligned} \quad (34)$$

Although this equation does not resemble the grand canonical equations, it is homogeneous in $\{g_{\mathbf{k}}\}$ and has far fewer terms.

In the case of an odd electron number $N_e = 2\nu + 1$, we define the fixed N_e wave function in terms of a residue integral as

$$|\Psi_{2\nu+1}\rangle = \frac{1}{2\pi i} \oint d\xi \xi^{-\nu-1} a_{\mathbf{q}\sigma}^\dagger \prod_{\mathbf{k} \neq \mathbf{q}} \left(1 + \xi g_{\mathbf{k}} a_{\mathbf{k}\uparrow}^\dagger a_{-\mathbf{k}\downarrow}^\dagger \right) |0\rangle. \quad (35)$$

This wave function carries a momentum label \mathbf{q} which gives the momentum of the unpaired electron (and hence of the total state). The normalization factor is now $\langle \Psi_{2\nu+1} | \Psi_{2\nu+1} \rangle = R_0^1(\mathbf{q})$, and the total energy is given by

$$\begin{aligned} E_{2\nu+1} = & \epsilon_{\mathbf{q}} + \sum_{\mathbf{k} \neq \mathbf{q}} \left(2\epsilon_{\mathbf{k}} - \frac{|U|}{N} \right) \frac{g_{\mathbf{k}}^2}{1 + g_{\mathbf{k}}^2} \frac{r_1^2(\mathbf{k}, \mathbf{q})}{r_0^1(\mathbf{q})} \\ & - \frac{|U|}{N} \sum_{\mathbf{k} \neq \mathbf{q}} \sum_{\mathbf{k}' \neq \mathbf{q}} \left[\frac{g_{\mathbf{k}}}{1 + g_{\mathbf{k}}^2} \frac{g_{\mathbf{k}'}}{1 + g_{\mathbf{k}'}^2} \frac{r_1^3(\mathbf{k}, \mathbf{k}', \mathbf{q})}{r_0^1(\mathbf{q})} \right. \\ & \left. + \frac{g_{\mathbf{k}}^2}{1 + g_{\mathbf{k}}^2} \frac{g_{\mathbf{k}'}^2}{1 + g_{\mathbf{k}'}^2} \frac{r_2^3(\mathbf{k}, \mathbf{k}', \mathbf{q})}{r_0^1(\mathbf{q})} \right]. \end{aligned} \quad (36)$$

This expression for the ground state energy has the same form as Eq. (28) except that the kinetic energy of the unpaired electron is singled out and the momentum sums explicitly prohibit the singly occupied momentum state. As in the even case a lengthy variational equation for the $g_{\mathbf{k}}$'s is obtained and must be solved numerically. The end result is that we have the ground state energy for any number of electrons.

Thus one can construct the gap by

$$2\Delta(N_e) \equiv E_{N_e-1} - 2E_{N_e} + E_{N_e+1}. \quad (37)$$

Various definitions of a gap or binding energy exist in the literature [22,19,8,21]. The basic idea is the same — one wants to compare the difference in energies between two systems, one in which $2N_e$ electrons are distributed equally over two subsystems containing N_e electrons each, and the other in which the subsystems contain

$N_e + 1$ and $N_e - 1$ electrons respectively. If N_e is even, the former has lower energy since pairing is fully utilized; this is reflected in a positive gap. If N_e is odd the latter has lower energy and therefore the gap is negative. This is the origin of the so-called parity effect measured by Tinkham and coworkers [1–3,16]. For evaluating the gap $\Delta(N_e)$ in Eq. (37), we choose the momentum \mathbf{q} that yields the lowest energy for a given odd number of electrons. This is important for properly recovering the exact results in certain regimes, i.e. strong coupling and/or low electron density.

In the grand canonical BCS formulation, there is a direct correspondence between the variational parameters and the occupation probability $n_{\mathbf{k}} \equiv \sum_{\sigma} \langle a_{\mathbf{k}\sigma}^\dagger a_{\mathbf{k}\sigma} \rangle$. It is determined through the $g_{\mathbf{k}}$'s as

$$n_{\mathbf{k}} = 2 \frac{g_{\mathbf{k}}^2}{1 + g_{\mathbf{k}}^2} = 1 - \frac{\epsilon_{\mathbf{k}} - \tilde{\mu}}{E_{\mathbf{k}}}, \quad (38)$$

where the various functions are defined in Section II B. Utilizing the $u_{\mathbf{k}}$'s and $v_{\mathbf{k}}$'s instead of the $g_{\mathbf{k}}$'s makes the correspondence even more transparent, for we have $n_{\mathbf{k}} = 2v_{\mathbf{k}}^2$ in that case. In the canonical formulation, for an even number of electrons, for example, we construct the matrix element

$$n_{\mathbf{k}\sigma} = \langle \psi_{2\nu} | a_{\mathbf{k}\sigma}^\dagger a_{\mathbf{k}\sigma} | \psi_{2\nu} \rangle, \quad (39)$$

and obtain

$$n_{\mathbf{k}} = \sum_{\sigma} n_{\mathbf{k}\sigma} = 2 \frac{g_{\mathbf{k}}^2}{1 + g_{\mathbf{k}}^2} r_1^1(\mathbf{k}). \quad (40)$$

2. Exact Solutions

The formalism developed so far is applicable in any dimension. The results to be discussed later in this paper focus on one dimension only. One reason is that the model is very local, so that for the properties we will discuss here, dimensionality is not too important. The second reason is that comparisons can be made with exact results, which are readily available only in one dimension.

Ground state energies can be obtained both by exact diagonalization (on small system sizes) and by Bethe Ansatz techniques [7,15,8]. We have already outlined in some detail [8] the numerical procedure used to obtain ground state energies for the attractive Hubbard model, and the reader is referred to those references for further details.

III. RESULTS

A. Ground state energy

We present results in one dimension and with only the nearest neighbours included for the electron hopping ($t_\delta \equiv t$). It has been shown in Ref. [8] that for large systems, the grand canonical BCS approximation yields the exact energy in the strong- and weak-coupling limits, and in the dilute limit for all coupling strengths. Thus deviations from the exact results are largest for weak to intermediate coupling strengths and for larger electron density $n \equiv \langle N_e \rangle / N$. We therefore anticipate improvements by the canonical BCS approximation for these cases, especially for small system size N . Because of the particle-hole symmetry [7,8], we need to study only up to half filling, $n = 1$ (i.e., the number of pairs is half the number of sites). Note that for the exact and canonical calculations, the density is defined simply by $n = N_e / N$ for a given number of electrons N_e . In the results shown below, for changing the density, we vary the electron number for a fixed system size, as is the case in the experiments.

In Fig. 1, we show the ground state energy per site (absolute value) as a function of the electron density for (a) $|U|/t = 10$ and 4 and $N = 16$, and for (b) $|U|/t = 2$ and $N = 4, 8$ and 32. The exact and canonical results are plotted with symbols and the grand canonical ones are shown with curves. In Fig. 1(a), for the exact and canonical cases, the energies with even and odd numbers of electrons are shown in different symbols. The conventional grand canonical BCS wave function contains only the components with even numbers of electrons. Strictly speaking, the exact and canonical results for odd numbers of electrons should be compared with the grand canonical ones in the parity-conserved scheme [18,23] with the odd number parity.

In Fig. 1(a), we first note the difference between the energies with even and odd numbers of electrons, as clearly seen for $|U|/t = 10$. The difference becomes more apparent for larger coupling strengths, giving rise to the even-odd oscillations in the energy as a function of the electron density. For $|U|/t = 10$, we note another difference between the even and odd electron numbers; the canonical energies are much closer to the exact ones for the even numbers. It can also be seen for this strong coupling case that the canonical results (for even N_e) are converged to the grand canonical ones for almost all density values, and both results are in very good agreement with the exact solutions for smaller density. As the coupling strength becomes smaller, for a fixed system size, the canonical energy deviates more from the grand canonical one and, for an even number of electrons, improves slightly the agreement with the exact energy for larger density. This can be seen for $|U|/t = 4$ in Fig. 1(a), while the even-odd difference is now smaller.

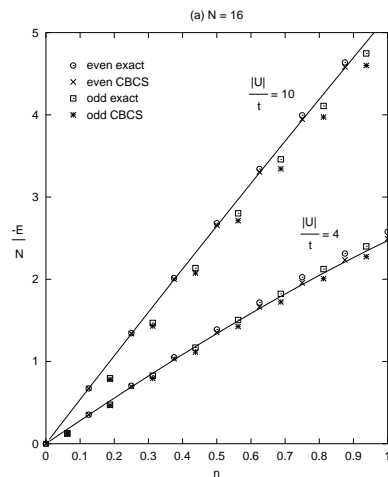


FIG. 1. (a) Ground state energy as a function of the electron density $n = N_e / N$ for 16 sites. The points are the canonical and exact results (different symbols for even and odd N_e), while the grand canonical ones are shown with curves. The difference between the energies with even and odd N_e can be seen clearly for $|U|/t = 10$. The canonical BCS results for even N_e are better than those for odd N_e , and converge to the grand canonical energies for strong coupling.

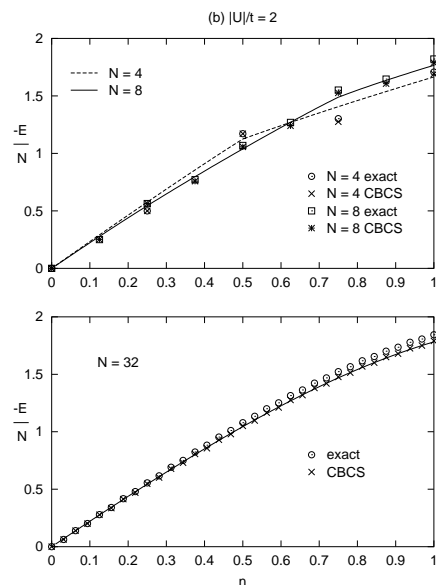


FIG. 1. (b) Same as (a), but for $|U|/t = 2$ and for $N = 4, 8$ (upper frame) and 32 (lower frame), and here the even and odd points are not distinguished. The improvement by the canonical scheme is more apparent for weak coupling and small system size, as can be seen for $N = 4$ and 8. For $N = 32$, the canonical and grand canonical results are more or less converged for all densities.

For smaller system size and coupling strength, we see more improvements due to the use of the canonical formulation. In the upper part of Fig. 1(b), we show the results for $|U|/t = 2$ and for $N = 4$ and 8. Note that the energy range is magnified compared with Fig. 1(a), and that for the exact and canonical results, the even and odd energies are not distinguished by different symbols. For $N = 4$ the agreement between the canonical and exact energies is excellent for all values of n , and it is still very good for $N = 8$. In the latter case, the grand canonical curve happens to be very close to the exact results for odd numbers of electrons for larger density. As explained above, however, the grand canonical results shown here must be compared for the even numbers only. In fact, the grand canonical energy for an even number of electrons differs most from the exact and canonical energies for larger density. On the other hand, the canonical energy converges to the grand canonical one as the system size becomes larger, as can be seen in Fig. 1(b) for $N = 32$. The even-odd difference is negligible for this weak coupling and large system size.

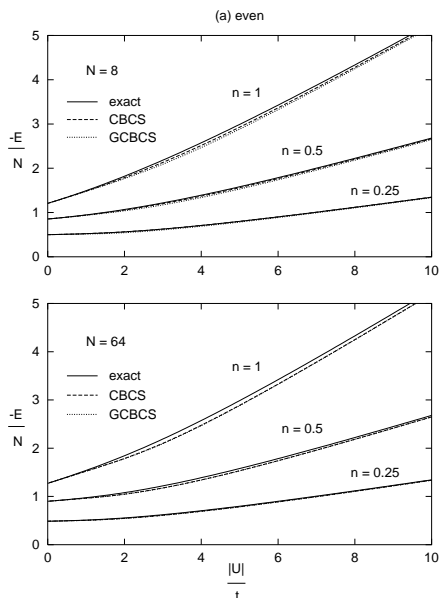


FIG. 2. (a) Ground state energy as a function of the coupling strength $|U|/t$ for $N = 8$ (upper frame) and 64 (lower frame) and for various values of $n = N_e/N$. For $N = 8$, the improvement by the canonical method can be seen, and for $n = 0.25$, the canonical and exact energies are indistinguishable. On the other hand, for $N = 64$, the canonical energies are converged to the grand canonical ones. Both the canonical and grand canonical results reproduce well the exact solutions for small n and in the zero- and strong-coupling limit.

In Fig. 2, the ground state energy is plotted as a function of the coupling strength for $N = 8$ and 64, for vari-

ous densities with (a) even and (b) odd numbers of electrons. For small systems, the canonical results improve the grand canonical ones, especially for intermediate coupling strengths, while the former converge to the latter as the coupling strength is increased. This can be seen for $N = 8$ in Fig. 2(a). In fact for $n = 0.25$, the exact (solid) and canonical (dashed) lines are indistinguishable, though the grand canonical one deviates from them only slightly. The three results converge as the coupling goes to zero, and also in the strong-coupling limit. For $N = 64$, the size is large enough that the canonical and grand canonical results are converged in the given scale for all densities and coupling strengths.

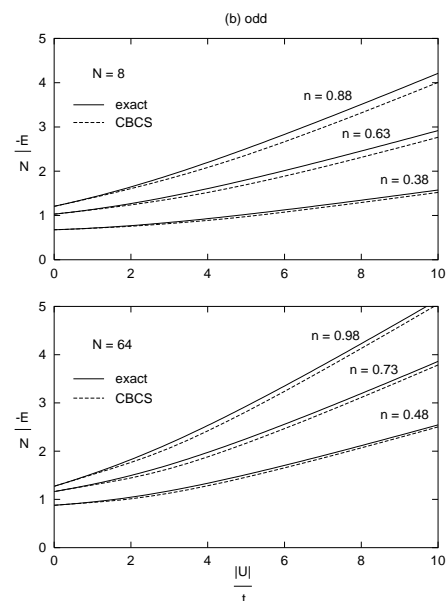


FIG. 2. (b) Same as (a), but here we compare the exact and canonical BCS results for an odd number of electrons N_e . For $N = 8$, the energies with odd N_e 's are poorly reproduced for large $|U|$ by the canonical BCS approximation, compared with the even- N_e case shown in (a). As the system size is increased, the difference between the errors in the energy for even and odd N_e 's becomes smaller, as can be seen for $N = 64$.

In Fig. 2(b), the canonical and exact energies are compared for odd electron numbers. For $N = 8$, compared with Fig. 2(a), the exact energy is reproduced rather poorly by the canonical BCS approximation, especially for larger coupling strengths. Moreover, unlike the even number case, the canonical BCS results do not converge to the exact ones as the coupling strength is increased further. This difference between the errors in the energy by the even- and odd- N_e canonical BCS approximation turns out to be smaller as the system size becomes larger. For $N = 64$, the difference between the even and odd cases has diminished significantly from the $N = 8$ case.

B. Energy gap

1. Finite size effects

We show the energy gap as a function of the density for (a) $|U|/t = 1$, (b) $|U|/t = 1.5$ and (c) $|U|/t = 4$; for $N = 4$ and 8 (upper figures) and $N = 16$ (lower figures) in Fig. 3 and for $N = 32$ (upper) and 64 (lower) in Fig. 4. Again, the exact and canonical results ($\Delta(N_e)$ in Eq. (37)) are plotted with symbols and the grand canonical results (Δ_o in Eq. (16)) are shown with curves. In the upper parts of Fig. 3, the exact solutions for $N = 4$ and 8 are the circles and squares, respectively, and the corresponding canonical results are the crosses and stars. The gaps for odd numbers of electrons are negative. As discussed above, the conventional BCS wave function that is used in this work does not contain the odd- N_e components, and thus the gap parameter defined by Eq. (16) misses out the gap for odd electron numbers. For even electron numbers, the canonical BCS method improves the grand canonical results significantly for weak coupling and small system size.

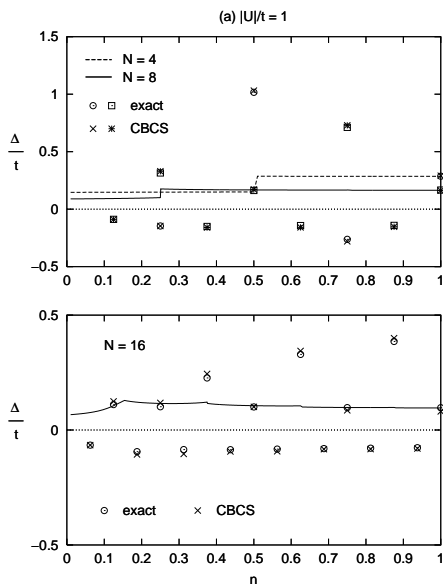


FIG. 3. (a) Energy gap as a function of the electron density $n = N_e/N$ for $N = 4, 8$ (upper frame) and 16 (lower frame) and for $|U|/t = 1$. In the upper figure, the circles and crosses are the exact and canonical BCS results for $N = 4$, respectively; the squares and stars are for $N = 8$. The grand canonical results are shown with curves. The gap for odd N_e is negative, and for even N_e , the *super-even* oscillations ($N_e = 4m$ vs. $4m + 2$) can be seen. The canonical results are in excellent agreement with the exact ones, while the grand canonical BCS result completely misses the gaps for $N_e = 4m + 2$.

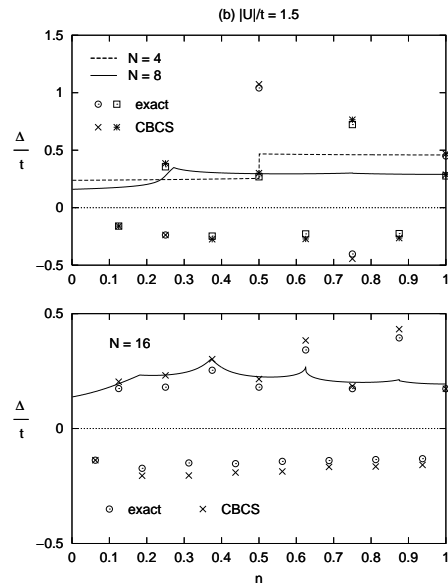


FIG. 3. (b) Same as (a), but for $|U|/t = 1.5$. The symbols used for the exact and canonical gaps for $N = 4$ and 8 are the same as in (a). The canonical results are still in good agreement with the exact ones.

In Fig. 3(a) for $|U|/t = 1$ and $N = 4, 8$ and 16, we can see the excellent agreement between the exact and canonical BCS results. Furthermore, there is a striking feature in these figures – the difference between the gaps for $N_e = 4m$ and $N_e = 4m + 2$, where m is an integer. (Note that for all the results shown, the number of sites is a multiple of four.) The gaps for $N_e = 4m + 2$ are much larger than those for $N_e = 4m$. Moreover, it is clearly seen for $N = 16$ that the gaps for $N_e = 4m + 2$ increase as the density increases. We call these oscillations in the gap as a function of the even- N_e the *super-even* effect: the system is more stable with $4m + 2$ electrons than with $4m$ electrons. This effect is more pronounced when the coupling is weak, and it stems from the quantized and doubly degenerate energy levels, $\epsilon_{\mathbf{k}} = \epsilon_{-\mathbf{k}}$, of the unperturbed system. As will be shown later, when the coupling is weak, the occupation probabilities of the unperturbed states can be approximated by those for zero coupling. We can thus understand the super-even effect as follows, in terms of the unperturbed energy levels which are occupied by pairs of electrons up to the Fermi level and are empty above it. To simplify the discussion, we ignore the energy change due to the blocked states by unpaired electrons.

In the case of one dimension and with $t_\delta = t$, the unperturbed energy, Eq. (2), reduces to $\epsilon_k = -2t \cos kR$, where R is the lattice constant. From the periodic boundary condition, $kR = 2\pi j/N$ ($-N/2 < j \leq N/2$), and

each energy level is degenerate for $\pm kR$ except for $kR = 0$ and π . Hence each level with $0 < |kR| < \pi$ can accommodate two pairs, $(k \uparrow, -k \downarrow)$ and $(-k \uparrow, k \downarrow)$. Thus when there are $4m + 2$ electrons, in the ground state, all the levels from $kR = 0$ up to kFR are fully occupied by the pairs, while with $4m$ electrons, the Fermi level has a vacancy for one more pair. Therefore, when there are $4m$ electrons, a way to break a pair with the minimum energy is to flip the spin of an electron of the pair at the Fermi level. The unpaired electrons then occupy the states $\pm k_F$ and there is no extra cost for the kinetic energy. On the other hand, when there are $4m + 2$ electrons, one cannot break either pair at the Fermi level simply by flipping a spin, but an unpaired electron has to move up to the next available level, increasing the kinetic energy. This is why the gap for pair breaking is larger for $4m + 2$ electrons than for $4m$ electrons. The fact that the former gap increases as a function of N_e is particular to the one-dimensional band structure that we use: the level spacing becomes maximum around $kR = \pi/2$ (i.e., half filling) and so does the kinetic energy cost for breaking a pair.

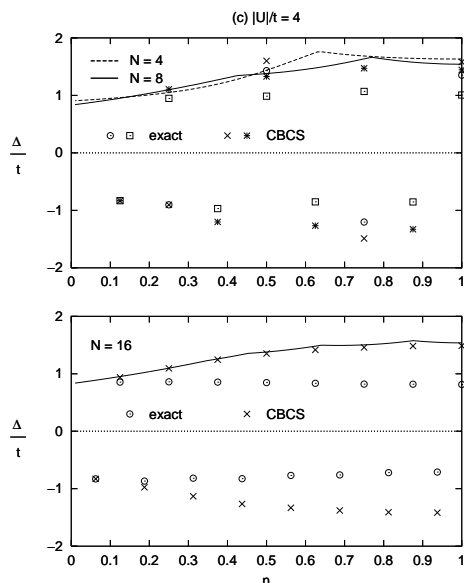


FIG. 3. (c) Same as (a), but for $|U|/t = 4$. For $N = 16$ the canonical gaps are converged to the grand canonical curve for almost all densities. Even for $N = 4$ and 8 , the canonical results are closer to the grand canonical ones, and the super-even oscillations have disappeared.

The super-even effect can be recognized more clearly in Fig. 4(a) for $N = 32$ and 64 . The overall scale of the gap becomes smaller for larger system size (note the reduced scale compared to Fig. 3(a)). For 32 sites, the canonical

BCS results still follow the exact solutions closely for almost all density values. For 64 sites, the system is so large that even for this weak coupling, the canonical gaps are converged to the grand canonical curve in the dilute limit. The canonical results more or less follow the exact ones for $n \gtrsim 0.3$, where the super-even effect is manifest.

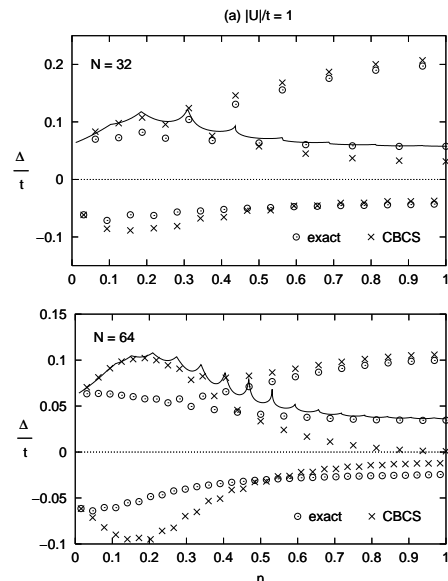


FIG. 4. (a) Same as Fig.3(a), but for larger system size; $N = 32$ (upper frame) and $N = 64$ (lower frame). The super-even oscillations can be seen clearly, whereas the grand canonical BCS misses the $4m + 2$ gaps completely. While for $N=32$ the canonical BCS results still follow the exact ones closely, for $N=64$ the former are closer to the grand canonical curve for low electron density.

It can be seen in Figs. 3(a) and 4(a) that for larger density, where the $4m$ and $4m + 2$ gaps are well separated, the grand canonical BCS completely misses the exact gaps for $N_e = 4m + 2$. On the other hand, the grand canonical curves appear to follow closely the exact $4m$ gaps. However, as the size is made larger than 64 sites, the exact $4m$ gaps become smaller than the gap given by the grand canonical curve (see the bottom graph of Fig. 4(a)) and finally in the bulk limit, they are quite small compared to the grand canonical values; at $n = 1.0$, the exact and grand canonical Δ/t are about 0.003 and 0.015 , respectively [8]. Meanwhile, the canonical $4m$ gaps go up towards the grand canonical curve, as they (and the $4m + 2$ gaps) converge to the grand canonical values. Hence for some particular sizes (larger than 64 sites), the canonical results for the $4m$ gaps will be closer to the exact ones.

In fact the grand canonical gaps tend to have a discon-

tinity at $N_e = 4m + 2$, but either value is generally well below the exact or canonical value. For smaller density where the super-even oscillations are not so prominent, the grand canonical gaps have cusps at $N_e = 4m + 2$, as can be seen, e.g., for $N = 64$ and $n \lesssim 0.5$ in Fig. 4(a). Also, as the coupling strength is made a little larger but still small ($|U|/t \lesssim 2$), these discontinuities at larger density are replaced by cusps. This can be seen in Figs. 3(b) and 4(b) for $|U|/t = 1.5$. While for the small sizes shown in Fig. 3(b) there are still discontinuities for $n \geq 0.5$, for the larger sizes in Fig. 4(b) the curves are continuous for all densities, with cusps at $N_e = 4m + 2$. It is intriguing that the grand canonical BCS partially reproduces the super-even oscillations in this way. The grand canonical solutions in the zero-coupling limit will be discussed further below.

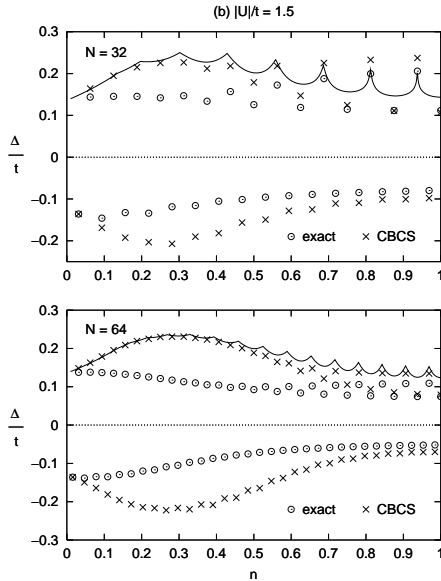


FIG. 4. (b) Same as (a), but for $|U|/t = 1.5$. The canonical gaps are converged to the grand canonical ones for smaller density, while the former improve the latter still significantly near half filling.

For $N = 4$ and 8 in Fig. 3(b), the agreement between the canonical and exact gaps is still very good, and the overall structure of the gaps as a function of the density is the same as for $|U|/t = 1$. For 16 sites, the canonical results deviate slightly but still reproduce the exact gaps well. For small density, the canonical even- N_e gaps are closer to the grand canonical curve, while for larger density the canonical $N_e = 4m + 2$ gaps significantly improve the grand canonical curve. As the system becomes larger, the super-even oscillations diminish in amplitudes and also are confined more towards half filling. Also, as

the size increases, for larger density where the (exact and canonical) $4m$ and $4m + 2$ gaps are well separated, the grand canonical curve shifts up relative to them, from near the $4m$ gaps to above the $4m + 2$ gaps. This can be seen in Figs. 3(b) and 4(b) in increasing order in size. For 32 sites, the last two cusps in the grand canonical curve happen to be closer to the exact values than the canonical ones. However, the canonical gaps capture the correct behaviour of the super-even oscillations. Finally for 64 sites, the canonical gaps are converged to the grand canonical one for low density, while they are much better for higher density, especially for $N_e = 4m$.

As the coupling strength is increased further (for a fixed size), the scale of the gap increases as a whole for both even and odd N_e (thus the even-odd difference becomes larger), while the $4m$ vs. $4m + 2$ difference decreases. For example, it can be seen in Figs. 3(c) and 4(c) that $|U|/t = 4$ is strong enough for most of the sizes shown for the system to reach the “bulk” limit, where the canonical and grand canonical methods hardly differ from one another. Even for $N = 4$ and 8 , the super-even structure is gone, and the canonical gaps are closer to the grand canonical ones.

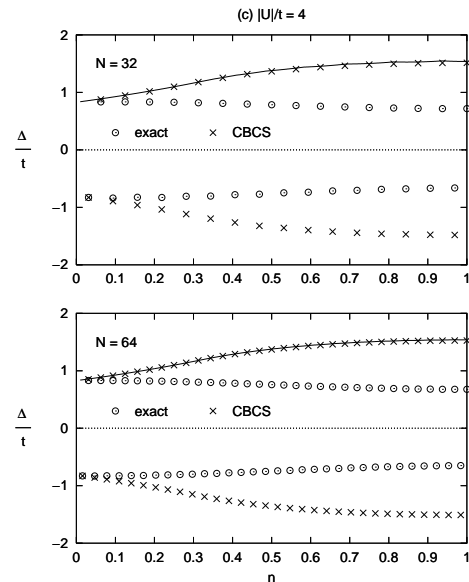


FIG. 4. (c) Same as (a), but for $|U|/t = 4$. For the large sizes shown, this is strong enough coupling so that the canonical and grand canonical results are converged for all densities, and the super-even oscillations have disappeared.

To see the effect of the coupling strength on the energy gap, we plot in Fig. 5(a) the gap as a function of the coupling strength for $N = 8$ (upper) and 64 (lower), for quarter ($n = 0.5$) and half filling. Interestingly, for $N = 8$

the exact gaps for quarter and half filling are almost the same for all $|U|$ values, whereas for $N = 64$ they are somewhat different. On the contrary, in the BCS picture (both canonical and grand canonical), the difference between quarter and half filling in the strong-coupling limit is about the same for small ($N = 8$) and large ($N = 64$) sizes and much larger than the exact result. As for the difference between the canonical and grand canonical results, we first note that $N_e = 4m$ for both cases shown in Fig. 5(a). For $N = 8$, the canonical and grand canonical results are equally good for weak coupling ($|U|/t \lesssim 2$), whereas the canonical gaps improve the grand canonical ones slightly for stronger coupling. For large systems and for very weak coupling, the grand canonical results are better than the canonical ones. This can be seen for $N = 64$ for $|U|/t \lesssim 1$ for half filling, as we have seen in Fig. 4(a). As the coupling becomes stronger, the canonical gap converges to the grand canonical one, and this happens faster for larger systems. Indeed for 64 sites, the two curves for $|U|/t \gtrsim 2$ can barely be distinguished in the given scale both for quarter and half filling, although half filling is a special case where the canonical gap defined by Eq. (37) does not converge to the conventional BCS gap – this will be discussed shortly.

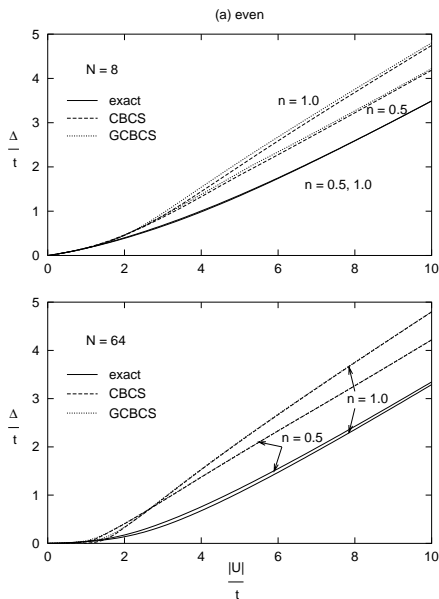


FIG. 5. (a) Energy gap as a function of the coupling strength $|U|/t$ for $N = 8$ (upper frame) and 64 (lower frame), for the densities $n = 0.5$ and 1.0 . For $N = 8$ (and for $N_e = 4m$) the canonical and grand canonical results are equally good for weak coupling, while the former improve the latter slightly for stronger coupling. For $N = 64$ the canonical and grand canonical results can hardly be distinguished for almost all the coupling strengths shown.

In Fig. 5(b), we compare the magnitude of the exact and canonical gaps for even and odd N_e for half filling, for 8 and 64 sites. For smaller systems, the magnitude of the gap for even $N_e (= 4m)$ is a little larger than the one for odd $N_e (= 4m \pm 1)$, as can be seen for $N = 8$. This difference is slightly larger for the exact solutions than the canonical BCS results. As the coupling strength or the system size is increased, this difference between the magnitude of the even ($4m$) and odd gaps diminishes. This can be seen in Fig. 5(b). Also note that the difference between the BCS gap and the exact gap increases as the system size increases. (This can be seen in Fig. 5(a) as well.) This is due to the fact that the exact gap becomes smaller for larger systems, whereas the canonical gap in the strong-coupling limit hardly changes as the system becomes larger (and $N = 64$ is large enough to be the bulk limit for $|U|/t \gtrsim 4$).

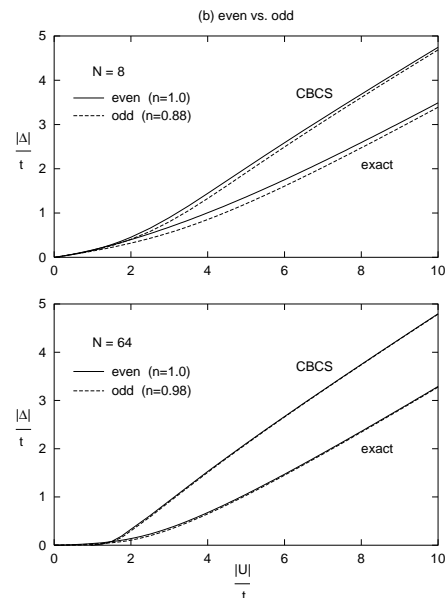


FIG. 5. (b) Same as (a), but here the magnitude of the gaps for even and odd electron numbers are compared for half filling, so that even $N_e = N$ and odd $N_e = N - 1$. For $N = 8$ the even gaps are slightly larger in magnitude than the odd ones, while for $N = 64$ the difference has diminished.

2. Grand canonical gap for weak coupling

As mentioned above, for very weak coupling, the grand canonical gaps have discontinuities for $N_e = 4m + 2$ at larger density. We can understand how these discontinuities arise, by looking at the density as a function of the chemical potential in the zero-coupling limit. In Fig. 6(a) we show the density (top) and the gap Δ_o (middle) as a

function of the chemical potential μ , and Δ_o as a function of the density n (bottom), for zero coupling and $N = 16$. When $|U| = 0$, $\Delta_{\text{BCS}} = 0$, $\tilde{\mu} = \mu$ and $E_k = |\epsilon_k - \mu|$. There is no gap equation and n is simply determined by Eq. (15) for a given μ . Thus the existence of a gap is solely due to the finite system size. It can be seen in the top figure that as μ changes continuously, the density n changes as a step function: it is multi-valued when μ is equal to any of the discrete ϵ_k due to the orbital and spin degeneracy. As μ moves from one level to the next, the density stays the same, whereas $\Delta_o = \min(E_k)$ increases from zero, peaks when μ is precisely between the two levels, and falls to zero again. Hence Δ_o as a function of n has δ -function-like peaks, as seen in the bottom figure.

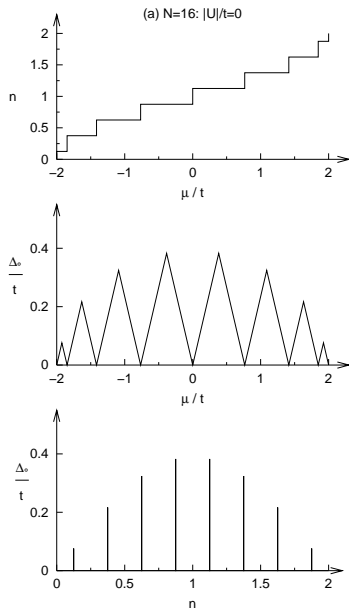


FIG. 6. (a) The electron density n (top frame) and the gap Δ_o (middle frame) as a function of the chemical potential μ , and Δ_o as a function of n (bottom frame), for $N = 16$ and for zero coupling. The fact that the density is a step function of μ and that the gap exists is because of quantized energy levels due to the finite system size. The Δ_o has peaks when $|\epsilon_k - \tilde{\mu}|$ becomes a maximum.

When the coupling is nonzero, n and μ must satisfy not only the number equation (15) but the gap equation

$$\frac{1}{|U|} = \frac{1}{N} \sum_{\mathbf{k}} \frac{1}{2 E_{\mathbf{k}}} = \frac{1}{N} \sum_{\mathbf{k}} \frac{1}{2 \sqrt{(\epsilon_{\mathbf{k}} - \tilde{\mu})^2 + \Delta_{\text{BCS}}^2}}, \quad (41)$$

which is obtained by substituting Eq. (14) into Eq. (12). It turns out that when the coupling is weak, $\tilde{\mu}$ given by Eq. (11) cannot take certain values in between two levels (corresponding to the plateau regions in n in Fig. 6(a)), and this can be understood in the following way.

For weak coupling, we can consider the relation between the density and chemical potential ($\tilde{\mu}$) roughly in the same way as for the zero-coupling case: for $N_e = 4m$, $\tilde{\mu}$ is very close to one of the levels ϵ_k (when $|U| = 0$, it is equal to ϵ_k), while for $N_e = 4m + 2$ it must be in between two levels. Therefore for $N_e = 4m$, $\epsilon_k - \tilde{\mu} \simeq 0$ and thus Δ_{BCS} must be finite for n to have a certain value (see Eq. (15)). For $N_e = 4m + 2$, however, if $\epsilon_k - \tilde{\mu}$ is finite, then Δ_{BCS} is driven to zero so that the RHS of Eq. (41) attains a large enough value for small $|U|$. Indeed, for sufficiently small $|U|$, even if Δ_{BCS} is zero, Eq. (41) *cannot* be satisfied for $\tilde{\mu}$ near the middle of the range between two levels. Instead $\tilde{\mu}$ is driven towards either level, so that the RHS of Eq. (41) increases sufficiently to equal the LHS. The number equation (15) is still satisfied, since $\Delta_{\text{BCS}} \simeq 0$. Thus certain values of $\tilde{\mu}$ are not allowed for small values of $|U|$. This situation is illustrated in Fig. 6(b) for $|U|/t = 1$. In the top part, the abrupt jumps in n seen in Fig. 6(a) have been somewhat smoothed, whereas the plateau parts have disappeared. Accordingly the gap becomes discontinuous as a function of $\tilde{\mu}$ as well as n . In the latter case, Δ_o indeed has two values for a given n at each discontinuity shown, corresponding to the two solutions for $\tilde{\mu}$ for coming up from a lower level and coming down from the next level. In any case, all values of n are possible (in contrast to $\tilde{\mu}$).

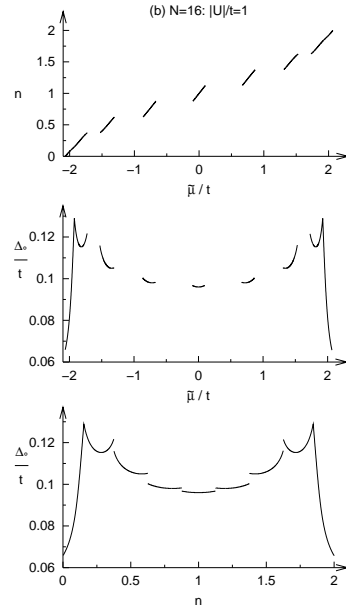


FIG. 6. (b) Same as (a), but for $|U|/t = 1$ and now the “chemical potential” is $\tilde{\mu}$ given by Eq. (11). The $\tilde{\mu}$ cannot take certain values in between unperturbed energy levels, corresponding to the plateau regions in (a).

For smaller density or larger system size, the level spacings become smaller, and it becomes possible for $\tilde{\mu}$ to

have all the values in between levels. This also occurs for stronger coupling, as can be seen in Fig. 6(c) for $|U|/t = 2$, where Δ_o is now continuous and has cusps at $N_e = 4m + 2$. These cusps come about when the coupling is still weak enough so that Δ_{BCS} is small, and for the same reason as in the zero-coupling case, that is, when $|\epsilon_k - \tilde{\mu}|$ becomes a maximum.

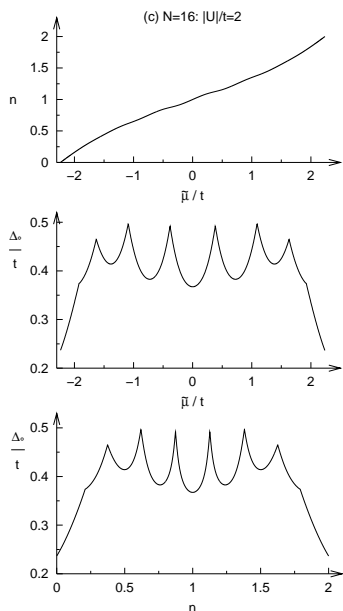


FIG. 6. (c) Same as (a), but for $|U|/t = 2$. This coupling strength is large enough so that $\tilde{\mu}$ can take all the values in between levels. On the other hand, the coupling is weak enough so that Δ_{BCS} is small, and Δ_o has cusps when $|\epsilon_k - \tilde{\mu}|$ becomes a maximum, similarly to the zero-coupling case.

It is intriguing that the weak but nonzero coupling picture described above does not interpolate smoothly to the zero-coupling case. As $|U|$ decreases, the slope of n (centred around $N_e = 4m$) as a function of $\tilde{\mu}$ seen in Fig. 6(b) (top frame) will become sharper, while the corresponding curves in $\Delta_o(\tilde{\mu})$ will be reduced to points. At exactly $|U| = 0$, n becomes vertical around $N_e = 4m$ for all m . However, all values of $\tilde{\mu}$ in between are allowed now, and $\Delta_o(\tilde{\mu})$ becomes continuous as in Fig. 6(a) (middle frame).

3. Quasi-particle energy

In the conventional BCS theory, there is no distinction between a particle- and a hole-excitation in that the energy $E_{\mathbf{k}} = \sqrt{(\epsilon_{\mathbf{k}} - \tilde{\mu})^2 + \Delta_{\text{BCS}}^2}$ is the same for either excitation [11]. As defined by Eq. (16), the gap Δ_o is the lowest quasi-particle energy $E_{\mathbf{k}}$. The minimum energy required for breaking a pair is $2\Delta_o$ and thus, the momenta

$|\mathbf{k}|$ carried by an electron and a hole are the same. In the canonical BCS scheme, for even N_e , the minimum pair-breaking energy is given by $2\Delta(N_e)$ in Eq. (37), where the lowest energy is chosen for each of the systems with $N_e - 1$, N_e , and $N_e + 1$ electrons. For the lowest E_{N_e+1} and E_{N_e-1} , the momentum carried by an unpaired electron and that by a hole, respectively, are not necessarily the same. (This is also the case for the exact solutions by the Bethe ansatz for a finite system.) In this section, we evaluate the gap $\Delta(N_e)$ by taking the same momentum for an electron and a hole as in the grand canonical picture, and compare it with the grand canonical quasi-particle energy. We should remark that the difference in gaps defined in these two different ways is generally quite small, but noticeable in certain extreme limits.

In Fig. 7, we plot $\Delta(N_e)$ obtained by the canonical BCS method, for which the same $|k|$ has been taken for an electron and a hole and which we call Δ_k , as a function of the kinetic energy ϵ_k . The energy band in one dimension is from $-2t$ to $2t$, corresponding to $0 \leq |kR| \leq \pi$. We show results for $N = 32$ and for quarter and half filling, i.e., $N_e = 16$ and $N_e = 32$, respectively; and for (a) $|U|/t = 1$, (b) $|U|/t = 5$ and (c) $|U|/t = 50$. The canonical results are shown with circles, while the grand canonical energy $E_{\mathbf{k}} = \sqrt{(\epsilon_{\mathbf{k}} - \tilde{\mu})^2 + \Delta_{\text{BCS}}^2}$ is plotted with solid curves.

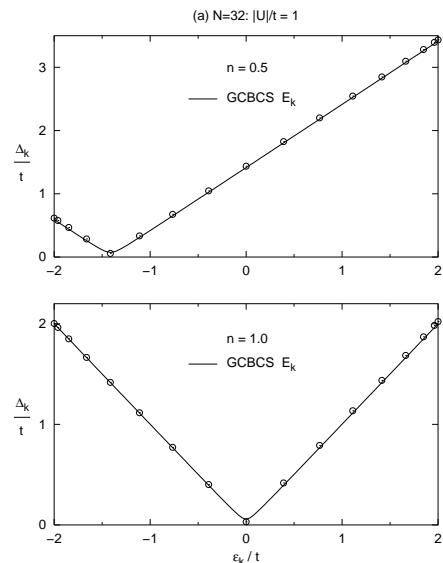


FIG. 7. (a) The momentum-dependent canonical gap Δ_k , for which the same $|k|$ is taken for an electron and a hole (circles), and the grand canonical quasi-particle energy E_k (curves), as a function of the kinetic energy ϵ_k . The results are for $N = 32$ and $|U|/t = 1$, and for quarter (upper frame) and half (lower frame) filling. For this weak coupling, $E_k \simeq |\epsilon_k - \tilde{\mu}|$.

We have seen in Fig. 4(a) that for $|U|/t = 1$ and $n \gtrsim 0.5$, the grand canonical gap (Δ_\circ) happens to be very close to the exact one for $N_e = 4m$, and for $N = 32$, also to the canonical gap (note that $N_e = 4m$ for both quarter and half filling). We also showed in Fig. 4(c) that $N = 32$ is large enough for the canonical gap to converge to the grand canonical BCS gap for almost the entire density range, already for $|U|/t = 4$. We find the result that the momentum-dependent canonical gap Δ_k defined in this section agrees remarkably well with the quasi-particle energy E_k (defined in the grand canonical context) for *all quasi-particle momenta* (i.e., not just at the minimum in Figs. 7(a)-(c)).

In the canonical picture, when the coupling is weak and there are $4m$ electrons, the lowest energy for breaking a pair is to create an electron and a hole both at the Fermi level. Thus $|k|$ for an electron and a hole is the same, and this explains the super-even effect. The gap with this configuration is the minimum value seen in Fig. 7(a) for both quarter and half filling. In the grand canonical scheme, Δ_{BCS} becomes very small for this weak coupling and hence $E_k \simeq |\epsilon_k - \tilde{\mu}|$, where $\tilde{\mu}$ turns out to be almost at the Fermi level (slightly above) for quarter filling and it is at the Fermi level for half filling ($\tilde{\mu} \equiv 0$).

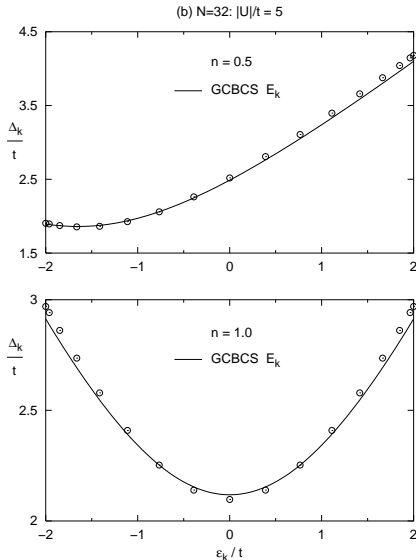


FIG. 7. (b) Same as (a), but for $|U|/t = 5$.

As the coupling strength increases, the momentum of an unpaired electron (or a hole) that yields the lowest energy for an odd N_e system shifts from the Fermi momentum in the zero-coupling limit towards zero momentum – it eventually reaches zero momentum, that is, the bottom of the non-interacting band, in the strong-coupling limit.

This happens sooner (i.e., for smaller $|U|$) for smaller number of electrons: not only the Fermi momentum for zero coupling is closer to zero than those for larger N_e , but also the optimal momentum starts shifting at weaker coupling. In the case of quarter filling for $N = 32$, the optimal momenta for $N_e = 15$ and 17 are both $|kR| = \pi/4$ for zero coupling, while for $|U|/t = 5$, the ground state energies E_{15} and E_{17} have different momentum dependence and have a minimum at $|kR| = 3\pi/16$ and $\pi/4$, respectively. Yet if we take the same momentum for both $N_e = 15$ and 17 , Δ_k agrees very well with E_k for all the $|k|$'s, as seen in Fig. 7(b). The Δ_k has its minimum when $E_{15} + E_{17}$ is the smallest; this occurs at $|kR| = 3\pi/16$ for $|U|/t = 5$. For half filling, the optimal momenta for both $N_e = 31$ and 33 are still $|kR| = \pi/2$ ($\epsilon_k = 0$) for $|U|/t = 5$, as in the zero-coupling case.

The preceding discussion illustrates that to obtain the grand canonical limit, one must in general choose the quasi-particle momentum (identical for the particle and hole cases) to minimize the sum of the two odd-electron energies. For intermediate to strong coupling this will not be given by the momentum expected from the non-interacting limit (in Ref. [9] this procedure worked because they adopted a particle-hole symmetric model – see below). The last case (next paragraph) shows this for a very strong coupling example.

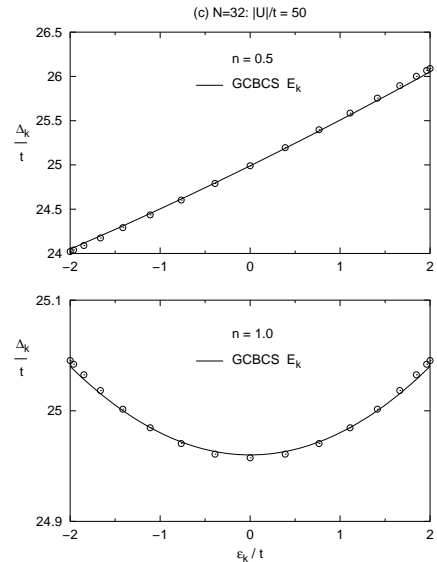


FIG. 7. (c) Same as (a), but for $|U|/t = 50$.

For extremely strong coupling such as $|U|/t = 50$, the optimal momenta for $N_e = 15$ and 17 are both zero. In such a case, the ground state energy increases almost linearly as a function of ϵ_k from $kR = 0$ to π . This can

be seen in the upper part of Fig. 7(d), where E_{15} and E_{17} are the squares (with the left axis) and the crosses (with the right axis), respectively. Accordingly, Δ_k is minimum at $kR = 0$ and increases linearly as a function of ϵ_k , as seen in Fig. 7(c). In the grand canonical case, $\tilde{\mu}$ (related to μ by Eq. (11)) for such strong coupling is a large negative value, and E_k has a minimum well below the bottom of the band.

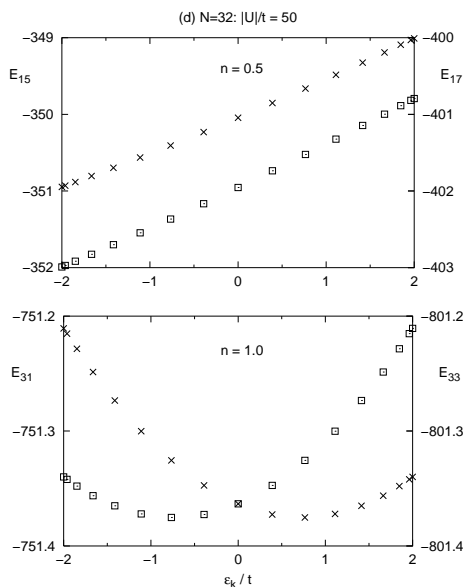


FIG. 7. (d) Ground state energy for odd N_e as a function of the quasi-particle kinetic energy ϵ_k , for $N = 32$. In the upper figure, the energies for $N_e = 15$ and 17 are shown with the squares (with the left axis) and the crosses (with the right axis), respectively; in the lower figure, the energies for $N_e = 31$ and 33 are plotted accordingly.

Half filling is a special case due to the particle-hole symmetry. In this case $\tilde{\mu}$ is zero for any coupling strength and hence the quasi-particle energy is always minimum at $|kR| = \pi/2$. By the canonical variation, the ground state energy for $N_e = 31$ (the largest odd number for $n \leq 1$) has its minimum at $3\pi/8$. This can be seen in the lower part of Fig. 7(d) (the squares, with the left axis), although the differences in energy for different $|k|$'s are rather small. The E_{33} (the crosses, with the right axis) is the mirror image of E_{31} about $|kR| = \pi/2$ as a function of the momentum (for any $|U|$), as follows from the particle-hole symmetry relation [7]. Interestingly, the optimal momentum for $N_e = 31$ (and for $N_e = 33$) is still close to $\pi/2$ for this coupling strength. Indeed, one requires even stronger coupling to have E_{31} that behaves like E_{15} in Fig. 7(d), while E_{33} will decrease in a symmetric fashion linearly from $kR = 0$ to π .

As the coupling increases, the system of any finite size approaches the “bulk” limit. We have seen above for $n = 0.5$ that in the strong-coupling limit, the energies for both of the odd systems (i.e., $N_e = 15$ and 17) have their minimum values with the momentum $k = 0$. This is true for any finite size and any density smaller than unity. Thus the canonical $\Delta(N_e)$ with the lowest E_{N_e+1} and E_{N_e-1} (N_e even) converges to Δ_o , which is, for such strong coupling, given by $\sqrt{(\epsilon_{\min} - \tilde{\mu})^2 + \Delta_{\text{BCS}}^2}$. This is not the case for half filling, however: the lowest E_{31} and E_{33} will have $kR = 0$ and π , respectively, while both should have $kR = \pi/2$ for the canonical gap to converge to Δ_o .

For $4m + 2$ electrons, the agreement of Δ_k with E_k is not as good for all quasi-particle momenta for weak coupling. In the strong-coupling limit, however, Δ_k eventually converges to E_k for all the momenta as we have seen above for $N_e = 4m$. Finally, as explained above for the super-even effect, the minimum gap for $N_e = 4m + 2$ for weak coupling has different $|k|$'s for the $N_e + 1$ and $N_e - 1$ systems. On the contrary, the grand canonical gap has always the same momentum for an electron and a hole. This explains why it does not reproduce the exact gap for $N_e = 4m + 2$ for such weak coupling, while the canonical one does.

C. Occupation probability

To conclude the discussion of our results, we show in Fig. 8(a) the variational parameter $\{g_k\}$ and (b) the occupation probability $\{n_k\}$ as a function of k and the coupling strength $|U|$, for $N = 8$ and 64 and for half filling. In both figures, the points at discrete values of k (and discrete values of $|U|$) are simply connected by lines. The smallest $|U|$ shown in these figures is $0.25t$, and for $N = 64$, the increment in $|U|$ has been taken finer than for $N = 8$ (while the k increment is naturally smaller for larger system size). The results shown have been obtained by the canonical BCS formalism. However, also in the grand canonical scheme, both $\{g_k\}$ and $\{n_k\}$ have the same overall shape as a function of k and $|U|$: the actual values of $\{g_k\}$ may be different but only slightly, so that they look the same as those in Fig. 8(a) in the given scale.

We can see in Fig. 8(a) that in the strong-coupling limit, $\{g_k\}$ as a function of k is almost flat (in the given scale) for a given $|U|$, and thus all the unperturbed levels are almost equally mixed [6]. On the other hand, in the zero-coupling limit, $\{g_k\}$ becomes a cosine function of k . Since the grand canonical BCS yields the same behaviour of $\{g_k\}$, this can be understood by the simple expression of Eq. (14). As $|U|$ approaches zero, Δ_{BCS} goes to zero, and E_k can be expanded up to the leading order in Δ_{BCS} . Then Eq. (14) reduces to

$$g_{\mathbf{k}} = \frac{1}{\Delta_{\text{BCS}}} \left[|\epsilon_{\mathbf{k}} - \tilde{\mu}| \left(1 + \frac{\Delta_{\text{BCS}}^2}{2(\epsilon_{\mathbf{k}} - \tilde{\mu})^2} \right) - (\epsilon_{\mathbf{k}} - \tilde{\mu}) \right]. \quad (42)$$

Thus in the limit of $|U| \rightarrow 0$ and $\Delta_{\text{BCS}} \rightarrow 0$,

$$g_{\mathbf{k}} \simeq \frac{\Delta_{\text{BCS}}}{2|\epsilon_{\mathbf{k}} - \tilde{\mu}|} \quad (\epsilon_{\mathbf{k}} > \tilde{\mu})$$

and

$$g_{\mathbf{k}} \simeq \frac{2|\epsilon_{\mathbf{k}} - \tilde{\mu}|}{\Delta_{\text{BCS}}} \quad (\epsilon_{\mathbf{k}} < \tilde{\mu}). \quad (43)$$

Hence $g_{\mathbf{k}} \rightarrow 0$ for $\epsilon_{\mathbf{k}} > \tilde{\mu}$, while for $\epsilon_{\mathbf{k}} < \tilde{\mu}$, $g_{\mathbf{k}}$ diverges in the zero-coupling limit, and provides an image of $\epsilon_{\mathbf{k}}$ (note that for half filling, $\tilde{\mu} = 0$).

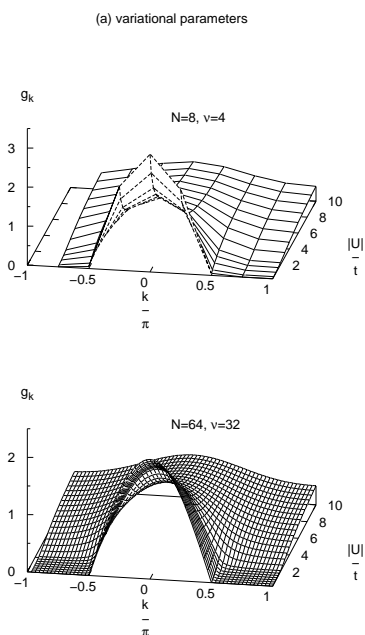


FIG. 8. (a) Variational parameter $\{g_{\mathbf{k}}\}$ as a function of k and the coupling strength $|U|/t$, for $N = 8$ (upper figure) and 64 (lower figure) and for half filling. The increment in $|U|/t$ has been taken to be finer for $N = 64$, while the increment in k is naturally smaller.

Furthermore, the occupation probability clearly shows how the distribution over the unperturbed states changes as a function of the coupling strength. It can be seen in Fig. 8(b) that the distribution function for the non-interacting case is recovered for weak coupling; $n_{\mathbf{k}} = 1$ for $\epsilon_{\mathbf{k}} < \tilde{\mu}$ and 0 for $\epsilon_{\mathbf{k}} > \tilde{\mu}$, and $n_{\mathbf{k}} = 0.5$ at the doubly degenerate Fermi level. In Fig. 8(b), not only the scale is reduced compared to Fig. 8(a), but also the relative (average) height of $n_{\mathbf{k}}$ at $|U|/t = 10$ against the one in the zero-coupling limit is larger. Thus $n_{\mathbf{k}}$ may appear to have more variation as a function of k in the strong-coupling limit than $g_{\mathbf{k}}$ does. However, the difference between the

maximum and minimum values at $|U|/t = 10$ are approximately the same for both cases, and $n_{\mathbf{k}}$ is about 0.7 at $k = 0$ and about 0.3 at the edges of the band. As the coupling is made stronger, the occupation probability (and $g_{\mathbf{k}}$) becomes almost equal for all the states, and $n_{\mathbf{k}} \simeq 0.5$ for all k in the case of half filling.

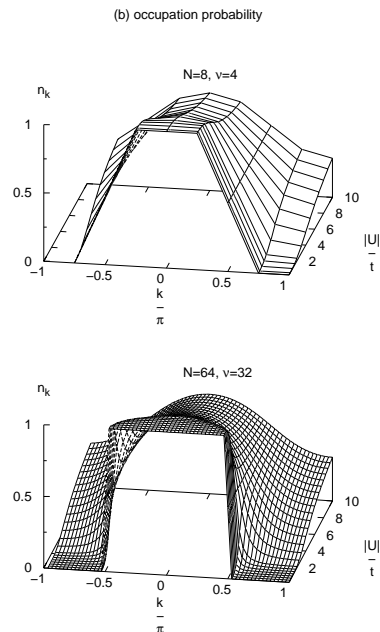


FIG. 8. (b) Occupation probability $\{n_{\mathbf{k}}\}$ as a function of k and $|U|/t$, for $N = 8$ (upper figure) and 64 (lower figure) and for half filling. At $|U|/t = 10$, $n_{\mathbf{k}}$ is roughly 0.7 and 0.3 at $k = 0$ and π , respectively (here the lattice constant $R \equiv 1$). In the weak-coupling limit, the distribution for the non-interacting electron gas is recovered.

IV. SUMMARY AND DISCUSSIONS

We have formulated BCS theory for a canonical ensemble, following earlier work by Dietrich *et al.* [12] and Falicov and Proetto [10], and very recently by Braun and von Delft [9]. We have also generalized the linear formulation introduced in Ref. [10] for any system size. However, this method has proven to be numerically too intensive for “large” systems, and provided at best only marginal improvement over the nonlinear canonical formulation.

In this work we have adopted a very definite model, the attractive Hubbard model, for various reasons. First, we wanted to have an exact solution with which to monitor the improvement over the grand canonical scheme. These are available for the Hubbard model in one dimension by the Bethe Ansatz technique, and so we have used these as a benchmark throughout this work. Second, we wanted to study a system which, by choice of parameters, could

easily span the weak coupling to strong coupling regime, as well as the low density to high density limits. In this way we have observed the crossover from the bulk to quantum limit for a variety of regimes. The attractive Hubbard model is no doubt the “minimal” model that accomplishes this. Finally, we wanted to use a model which could readily be generalized to a realistic case, so, for example, one could use a parametrized tight-binding model to fit the band structure for Al to better describe ultrasmall metallic Al grains.

In this work, however, we focused on the first two points listed above, with the goal of establishing generic trends. The existence of the parity effect, as already determined by a parity-projected grand canonical scheme [18,23] and more recently by the canonical formulation of a uniformly-spaced-level model [9], emerges quite naturally in this model. However, in addition to the even-odd effect, we have found a *super-even* effect, with oscillations in the superconducting gap occurring between even electron numbers which are multiples of 4 ($4m$) and non-multiples of 4 ($4m + 2$). The magnitude of the gap variation for even numbers of electrons is, in some cases, comparable to the even-odd variation, i.e. $|\Delta(4m) - \Delta(4m + 1)| \approx |\Delta(4m) - \Delta(4m + 2)|$. Thus, such oscillations should be observable in the same kind of tunneling experiments for seeing the even-odd effect. We note, however, a key ingredient for the super-even effect to occur is the double degeneracy of levels, which in our case comes about from the simple equality, $\epsilon_{\mathbf{k}} = \epsilon_{-\mathbf{k}}$. In a more general case, the degeneracy structure will be more complicated, and therefore oscillations will exist but may not be as simply periodic as a function of electron number as is the case here. The super-even effect is also a result of quantized energy levels due to finite system size, and the effect will be stronger for smaller systems. For very weak coupling, the grand canonical BCS fails to reproduce the super-even effect, while the canonical scheme does; indeed, it yields very good agreement with the exact solutions.

Finally, we note that the grand canonical BCS quasiparticle dispersion relation was beautifully reproduced by the canonical results, *simply by varying the odd number ground state momentum*, with the proviso that the electron and hole momenta were the same. This simple correspondence is quite surprising.

ACKNOWLEDGMENTS

This research was supported by the Avadh Bhatia Fellowship and by the Natural Sciences and Engineering Research Council of Canada and the Canadian Institute for Advanced Research. We are grateful to Bob Teshima for his help in efficiently evaluating the residue integrals using the analytical results. K.T. thanks Rajat Bhaduri, Jules Carbotte and Elisabeth Nicol for helpful comments

and discussions. Calculations were performed on the 42 node SGI parallel processor at the University of Alberta.

APPENDIX: LINEAR CANONICAL VARIATION

We summarize the linearized formulation of the canonical variation. In addition to the wave function for $N_e = 2\nu$ defined by Eq. (18), we define the wave function for odd number of electrons $N_e = 2\nu + 1$, following [8] as

$$|\Psi_{2\nu+1}\rangle = a_{\mathbf{q}\sigma}^\dagger \sum_{\mathbf{k}_1 \neq \mathbf{q} < \mathbf{k}_2 \neq \mathbf{q} < \dots < \mathbf{k}_\nu \neq \mathbf{q}} C(\mathbf{k}_1, \mathbf{k}_2, \dots, \mathbf{k}_\nu) \times \prod_{i=1}^{\nu} a_{\mathbf{k}_i \uparrow}^\dagger a_{-\mathbf{k}_i \downarrow}^\dagger |0\rangle, \quad (\text{A1})$$

where spin of the extra electron σ can be either up or down. The extra electron blocks the state \mathbf{q} from being occupied by pairs. There is no variational parameter for the blocked state: for the variational calculations, we always choose \mathbf{q} that gives the lowest energy. Note that the C 's in the above equation are different from those for the same number of pairs in Eq. (18) due to the missing \mathbf{q} .

We now derive the variational equation using $|\Psi_\nu\rangle$ in Eq. (18) for an even number of electrons $N_e = 2\nu$. The formulae below are slightly modified for an odd number of electrons $N_e = 2\nu + 1$ in terms of the odd wave function (A1). We mention the difference for $N_e = 2\nu + 1$ in the end.

The normalization factor for $|\Psi_{2\nu}\rangle$ defined in Eq. (18) is

$$\begin{aligned} \langle \Psi_{2\nu} | \Psi_{2\nu} \rangle &= \sum_{\mathbf{k}_1 < \dots < \mathbf{k}_\nu} \sum_{\mathbf{p}_1 < \dots < \mathbf{p}_\nu} C^*(\mathbf{k}_1, \dots, \mathbf{k}_\nu) C(\mathbf{p}_1, \dots, \mathbf{p}_\nu) \\ &\times \langle 0 | a_{-\mathbf{k}_\nu \downarrow} a_{\mathbf{k}_\nu \uparrow} \dots a_{-\mathbf{k}_1 \downarrow} a_{\mathbf{k}_1 \uparrow} \\ &\quad a_{\mathbf{p}_1 \uparrow}^\dagger a_{-\mathbf{p}_1 \downarrow}^\dagger \dots a_{\mathbf{p}_\nu \uparrow}^\dagger a_{-\mathbf{p}_\nu \downarrow}^\dagger |0\rangle \\ &= \sum_{\mathbf{k}_1 < \dots < \mathbf{k}_\nu} |C(\mathbf{k}_1, \dots, \mathbf{k}_\nu)|^2. \end{aligned} \quad (\text{A2})$$

Similarly, the expectation value of the kinetic energy operator in $H = \hat{T} + \hat{V}$ is

$$\begin{aligned} \langle \Psi_{2\nu} | \hat{T} | \Psi_{2\nu} \rangle &= \langle \Psi_{2\nu} | \sum_{\mathbf{k}\sigma} \epsilon_{\mathbf{k}} a_{\mathbf{k}\sigma}^\dagger a_{\mathbf{k}\sigma} | \Psi_{2\nu} \rangle \\ &= \sum_{\mathbf{k}_1 < \dots < \mathbf{k}_\nu} |C(\mathbf{k}_1, \dots, \mathbf{k}_\nu)|^2 2(\epsilon_{\mathbf{k}_1} + \dots + \epsilon_{\mathbf{k}_\nu}). \end{aligned} \quad (\text{A3})$$

Calculation of the potential energy term is more tedious. After some lengthy operator algebra it can be written in a general form for ν pairs as

$$\begin{aligned}
 & \langle \Psi_{2\nu} | \hat{V} | \Psi_{2\nu} \rangle \\
 &= -\frac{|U|}{N} \langle \Psi_{2\nu} | \sum_{\mathbf{k}\mathbf{k}'1} a_{\mathbf{k}\uparrow}^\dagger a_{-\mathbf{k}+1\downarrow}^\dagger a_{-\mathbf{k}'+1\downarrow} a_{\mathbf{k}'\uparrow} | \Psi_{2\nu} \rangle \\
 &= -\frac{|U|}{N} \sum_{\mathbf{k}_1 <} \cdots \sum_{< \mathbf{k}_\nu} C(\mathbf{k}_1, \cdots, \mathbf{k}_\nu) \\
 &\times \left[\nu(\nu-1) C^*(\mathbf{k}_1, \cdots, \mathbf{k}_\nu) \right. \\
 &+ \sum_{\mathbf{p} < \mathbf{k}_1} C^*(\mathbf{p}, \mathbf{k}_1, \mathbf{k}_2, \cdots, \mathbf{k}_{\nu-1}) \\
 &+ \sum_{\mathbf{k}_1 < \mathbf{p} < \mathbf{k}_2} C^*(\mathbf{k}_1, \mathbf{p}, \mathbf{k}_2, \cdots, \mathbf{k}_{\nu-1}) \\
 &+ \cdots + \sum_{\mathbf{k}_{\nu-1} < \mathbf{p}} C^*(\mathbf{k}_1, \mathbf{k}_2, \cdots, \mathbf{k}_{\nu-1}, \mathbf{p}) \\
 &+ \sum_{\mathbf{p} < \mathbf{k}_1} C^*(\mathbf{p}, \mathbf{k}_1, \mathbf{k}_2, \cdots, \mathbf{k}_{\nu-2}, \mathbf{k}_\nu) \\
 &+ \sum_{\mathbf{k}_1 < \mathbf{p} < \mathbf{k}_2} C^*(\mathbf{k}_1, \mathbf{p}, \mathbf{k}_2, \cdots, \mathbf{k}_{\nu-2}, \mathbf{k}_\nu) \\
 &+ \cdots + \sum_{\mathbf{k}_\nu < \mathbf{p}} C^*(\mathbf{k}_1, \mathbf{k}_2, \cdots, \mathbf{k}_{\nu-2}, \mathbf{k}_\nu, \mathbf{p}) \\
 &+ \cdots \\
 &+ \sum_{\mathbf{p} < \mathbf{k}_2} C^*(\mathbf{p}, \mathbf{k}_2, \mathbf{k}_3, \cdots, \mathbf{k}_\nu) \\
 &+ \sum_{\mathbf{k}_2 < \mathbf{p} < \mathbf{k}_3} C^*(\mathbf{k}_2, \mathbf{p}, \mathbf{k}_3, \cdots, \mathbf{k}_\nu) \\
 &+ \cdots + \left. \sum_{\mathbf{k}_\nu < \mathbf{p}} C^*(\mathbf{k}_2, \mathbf{k}_3, \cdots, \mathbf{k}_\nu, \mathbf{p}) \right] \quad (\text{A4})
 \end{aligned}$$

The first term on the right hand side corresponds to a Hartree-like term, and gives the interaction energy of each of the ν pairs with the other $\nu-1$ pairs. The other terms systematically consider the various cases when one pair is scattered into another (unoccupied) pair state.

In the following, we take the C 's to be real variables. In Ref. [12] it has been proved for the BCS formulation that for negative pairing-type interactions, real (and positive) variational parameters yield the lowest energy. The minimization condition for the energy (20) with respect to the real $\{C\}$ results in the equation

$$\begin{aligned}
 C(\mathbf{k}_1, \cdots, \mathbf{k}_\nu) &= -\frac{1}{d} \frac{|U|}{N} \left[\sum_{\mathbf{p} < \mathbf{k}_1} C(\mathbf{p}, \mathbf{k}_1, \mathbf{k}_2, \cdots, \mathbf{k}_{\nu-1}) \right. \\
 &+ \sum_{\mathbf{k}_1 < \mathbf{p} < \mathbf{k}_2} C(\mathbf{k}_1, \mathbf{p}, \mathbf{k}_2, \cdots, \mathbf{k}_{\nu-1}) \\
 &+ \cdots + \sum_{\mathbf{k}_{\nu-1} < \mathbf{p} \neq \mathbf{k}_\nu} C(\mathbf{k}_1, \mathbf{k}_2, \cdots, \mathbf{k}_{\nu-1}, \mathbf{p}) \\
 &+ \sum_{\mathbf{p} < \mathbf{k}_1} C(\mathbf{p}, \mathbf{k}_1, \mathbf{k}_2, \cdots, \mathbf{k}_{\nu-2}, \mathbf{k}_\nu) \\
 &+ \sum_{\mathbf{k}_1 < \mathbf{p} < \mathbf{k}_2} C(\mathbf{k}_1, \mathbf{p}, \mathbf{k}_2, \cdots, \mathbf{k}_{\nu-2}, \mathbf{k}_\nu)
 \end{aligned}$$

$$\begin{aligned}
 &+ \cdots + \sum_{\mathbf{k}_{\nu-2} < \mathbf{p} \neq \mathbf{k}_{\nu-1} < \mathbf{k}_\nu} C(\mathbf{k}_1, \mathbf{k}_2, \cdots, \mathbf{k}_{\nu-2}, \mathbf{p}, \mathbf{k}_\nu) \\
 &+ \sum_{\mathbf{k}_\nu < \mathbf{p}} C(\mathbf{k}_1, \mathbf{k}_2, \cdots, \mathbf{k}_{\nu-2}, \mathbf{k}_\nu, \mathbf{p}) \\
 &+ \cdots \\
 &+ \sum_{\mathbf{p} \neq \mathbf{k}_1 < \mathbf{k}_2} C(\mathbf{p}, \mathbf{k}_2, \mathbf{k}_3, \cdots, \mathbf{k}_\nu) \\
 &+ \sum_{\mathbf{k}_2 < \mathbf{p} < \mathbf{k}_3} C(\mathbf{k}_2, \mathbf{p}, \mathbf{k}_3, \cdots, \mathbf{k}_\nu) \\
 &+ \cdots + \sum_{\mathbf{k}_\nu < \mathbf{p}} C(\mathbf{k}_2, \mathbf{k}_3, \cdots, \mathbf{k}_\nu, \mathbf{p}) \left. \right], \quad (\text{A5})
 \end{aligned}$$

where

$$d = E_\nu - 2(\epsilon_{\mathbf{k}_1} + \cdots + \epsilon_{\mathbf{k}_\nu}) + \frac{|U|}{N} \nu^2. \quad (\text{12}')$$

This should be solved for all the C 's selfconsistently.

For an odd number of electrons, in the energy expectation value and the variational equation in terms of $|\Psi_{2\nu+1}\rangle$, the blocked \mathbf{q} is excluded in all the $\{\mathbf{k}\}$ sums and $\{\mathbf{p}\}$ sums. Other than that, the normalization factor for $|\Psi_{2\nu+1}\rangle$ is the same as Eq. (A2): the kinetic energy term is the same as Eq. (A3) except that $2(\epsilon_{\mathbf{k}_1} + \cdots + \epsilon_{\mathbf{k}_\nu})$ should be replaced by $2(\epsilon_{\mathbf{k}_1} + \cdots + \epsilon_{\mathbf{k}_\nu}) + \epsilon_{\mathbf{q}}$: the potential energy term is the same as Eq. (A4) except that the factor $\nu(\nu-1)$ should be replaced by ν^2 : the variational equation is the same as Eq. (A5), while in d as defined in Eq. (A6) $-\epsilon_{\mathbf{q}}$ should be added and ν^2 should be replaced by $\nu(\nu+1)$.

We have found that this linear variation in terms of the C 's just barely improves the ground state energy, compared to the nonlinear variation in terms of the g 's. Interestingly, the C -formulation does not improve the g -formulation for the energy gap. We illustrate this in Fig. 9 for $N = 16$ and for $|U|/t = 1.5$ and 4. We found that for smaller system size, the two formulations do not make any difference for any coupling strength, for the gap as well as the ground state energy. For larger system size (which was limited for $N \lesssim 30$) the gap from the C -formulation is slightly worse than the one from the g -formulation for weak coupling and larger density. This can be seen in Fig. 9(a), while for $|U|/t = 4$ in (b) the two results have converged for all the density.

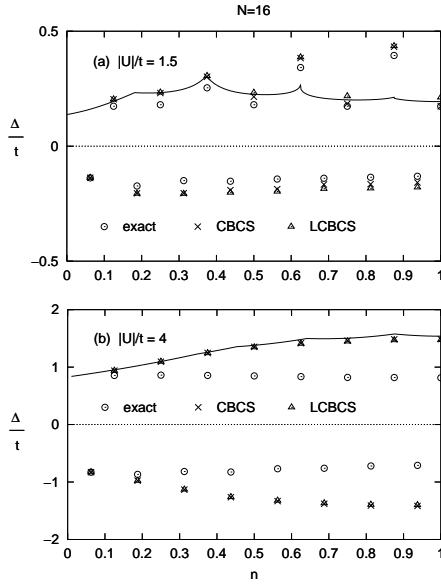


FIG. 9. Energy gap as a function of the electron density n for $N = 16$, for (a) $|U|/t = 1.5$ and (b) $|U|/t = 4$. The exact solutions are shown with circles, while the canonical results from the g -formulation and from the linear C -formulation are shown with the crosses and triangles, respectively.

- [14] P. Ring and P. Schuck, *The Nuclear Many-Body Problem* (Springer-Verlag, New York, 1980).
- [15] T. B. Bahder and F. Woyнарovich, Phys. Rev. B **33**, 2114 (1986).
- [16] M. T. Tuominen, J. M. Hergenrother, T.S. Tighe and M. Tinkham, Phys. Rev. Lett. **69**, 1997 (1992).
- [17] P. Lafarge, P. Joyez, D. Esteve, C. Urbina and M. H. Devoret, Phys. Rev. Lett. **70**, 994 (1993).
- [18] B. Jankó, Anders Smith and V. Ambegaokar, Phys. Rev. B **50**, 1152 (1994).
- [19] R. M. Fye, M. J. Martins and R. T. Scalettar, Phys. Rev. B **42**, 6809 (1990).
- [20] F. Braun and J. von Delft, cond-mat/9801170.
- [21] K. A. Matveev and A. I. Larkin, Phys. Rev. Lett. **78**, 3749 (1997).
- [22] J. E. Hirsch, S. Tang, E. Loh, Jr., and D. J. Scalapino, Phys. Rev. Lett. **60**, 1668 (1988).
- [23] F. Braun, J. von Delft, D. C. Ralph, and M. Tinkham, Phys. Rev. Lett. **79**, 921 (1997).

- [1] D. C. Ralph, C. T. Black and M. Tinkham, Phys. Rev. Lett. **74**, 3241 (1995).
- [2] C. T. Black, D. C. Ralph and M. Tinkham, Phys. Rev. Lett. **76**, 688 (1996).
- [3] D. C. Ralph, C. T. Black and M. Tinkham, Phys. Rev. Lett. **78**, 4087 (1997).
- [4] P. W. Anderson, J. Phys. Chem. Solids **11**, 26 (1959).
- [5] J. Bardeen, L.N. Cooper and J.R. Schrieffer, Phys. Rev. **108**, 1175 (1957)
- [6] P. Nozières and S. Schmitt-Rink, J. Low Temp. Phys. **59**, 195 (1985).
- [7] E. H. Lieb and F. Y. Wu, Phys. Rev. Lett. **20**, 1445 (1968).
- [8] F. Marsiglio, Phys. Rev. B **55**, 575 (1997).
- [9] F. Braun and J. von Delft, Phys. Rev. Lett. **81**, 4712 (1998).
- [10] L. M. Falicov and C. R. Proetto, Phys. Rev. B **47**, 14407 (1993).
- [11] J. R. Schrieffer, *Theory of Superconductivity* (Benjamin/Cummings, Don Mills, 1964).
- [12] K. Dietrich, H. J. Mang and J. H. Pradal, Phys. Rev. **135**, B22 (1964).
- [13] B. F. Bayman, Nuc. Phys. **15**, 33 (1960).